TPG4920: Petroleum Engineering, master's Thesis

Master Thesis

Masolwa Kasongi Enos

Evaluation of Models to Predict Liquid Loading in Gas wells

Trondheim-Norway, August 2018

Supervisor: Prof Milan Stanko (NTNU)

Co-Supervisor: Dr Karim Baruti (UDSM)

NTNU
Norwegian University of Science and Technology
Faculty of Engineering
Department of Geoscience and Petroleum

NTNU

Abstract

Liquid production in the form of water or condensate is essentially the most common problem in mature gas wells. For efficient operation of the well, the produced liquid must be continuously transported to the surface. This is only possible when gas rate is above a certain threshold known as the critical velocity. With depletion, gas rate declines, when it reaches below the critical velocity, liquid starts to accumulate at the bottom of the well creating what is referred to as liquid loading. Liquid loading causes a rapid gas rate decline, reduces the ultimate recovery of a gas well and may completely kill the well if immediate liquid unloading actions are not taken. Several models have been devised to predict the inception of liquid loading. Some models are based on the liquid droplet reversal and others are based on the liquid film reversal. However, each model provides divergent views on the critical gas velocity required to initiate liquid loading. Some models under- predicts while others over-predicts the critical gas velocity.

In the present work, the liquid droplet model of Turner et al. (1969) and the liquid film reversal models of Barnea (1986,1987), Luo et al. (2014) and Shekhar et al. (2017) were compared against the field data available in the literatures. It was observed that the Turner's model can accurately predict the onset of liquid loading and the loading status of gas wells producing under unloaded conditions while the model was found to under-estimate the critical velocity for wells producing under loaded condition. It was also observed that, out of all film reversal models compared, the Shekhar et al. (2017) model can better predict the critical velocity especially for deviated wells with large diameters in the range of 2 to 6 inches.

The study on the effect of droplet entrainment in the film reversal models have revealed that the film reversal models can over-estimate the critical velocity by up to 18% if the fraction of droplets entrainment is neglected in the models. The Shekhar et al. (2017) model was therefore modified to incorporate the Oliemans et al. (1986) entrainment correlation instead of the Wallis (1969) correlation used in the Luo et al. (2014) model. The results were found to be better than the original Shekhar et al. (2017) model without droplet entrainment while that of Luo's model were conservative. The study on the liquid loading criteria along the wellbore have revealed that both the wellhead and the bottomhole should be used as the evaluation point of the critical gas velocity so that a precise conclusion of whether the well is loaded or unloaded could be drawn.

Acknowledgments

I would like to extend my sincere hand of gratitude to Almighty God for his unlimited blessings that He bestowed to me all the time during execution of this project. It has been a great pleasure to me to get an opportunity to pursue a master's degree at the Norwegian university of Science and Technology (NTNU). I would like to acknowledge Equinor for making this possible through their financial support.

My special thanks should go to my supervisor, Prof. Milan Stanko for his close guidance throughout this thesis. I am very glad to have such a great supervisor and I do appreciate him for taking his time in counseling, conversation, and timely response to any of my queries all the time when I sent him the requests. His structured thinking and willing to combat the problem of liquid loading in gas wells have encouraged me to deepen and focus on improving the models used to predict the onset of liquid loading so that early plans should be made during the design phase on the optimal ways to unload the liquid when the problem arises. I would also like to appreciate the contribution from my Co-supervisor Dr Karim Baruti from the university of Dar es Salaam for his advice and support on the structure of the report.

Finally, I would like to appreciate my wife Sofia and our baby born Elina for their patience to sometimes allow me to work outside the study hours. Their support and encouragement have been the reasons of my happiness. I do recognize My parents, brothers, Sisters and all colleagues who have been motivating me to work hard in my studies.

TABLE OF CONTENTS

List of Figures

List of Tables

1.0 INTRODUCTION

Most gas wells produce liquid which flows along with gas as droplets entrained in gas stream or as films flowing along the walls of a tubing. The produced liquid may originate from interstitial water in the reservoir matrix or condensation of hydrocarbon gas (condensate). As soon as gas wells are drilled, gas rates are usually high enough to lift all the produced liquids to the surface. As the reservoir pressure declines with depletion, the gas production rate also decreases until the current gas rate is unable to lift the produced liquids to the surface. The produced liquids then start to accumulate at the bottom of the well (sandface) creating a static column of liquid. This causes the bottomhole pressure to increase and create the back pressure against the formation which affect the production capacity of the well.

Continuous accumulation of liquid in the well increases the saturation of liquids and reduces the effective permeability close to the wellbore which in turn reduces the gas production rate. For low pressure gas wells, the well may eventually die, while for high pressure gas wells, liquid loading may facilitate slugging or churning of liquids that would affect the well test calculations, which usually assumes continuous removal of liquids.

Different scholars have suggested several models to predict the inception of liquid loading in gas wells. The proposed models are either based on the liquid droplet reversal or liquid film reversal. Turner et al. (1969) proposed a model based on the droplet reversal, this model was found to better predict the liquid loading condition especially for vertical unloaded wells, though some already loaded wells could not be covered even after a 20% upward adjustment (Zhou & Yuan, 2010). Coleman et al. (1991) observed that, a 20% upward adjustment recommended by Turner et al. was not necessary for low rate gas wells and Wellhead flowing pressure (WHFP) below 500 psia (Riza et al. 2016). There are different modifications to the Turner's model such as the Nosseir et al. (2000), Belfroid et al. (2008), Veeken et al. (2010) and Sutton et al. (2010). However, some experimental studies have observed that, liquid loading is caused by liquid film reversal instead of the liquid droplet reversal.

Barnea (1986, 1987) and Zhang et al.(2003a) suggested models based on the liquid film reversal hypothesis for vertical and inclined wells. The models use the transition boundary from annular to slug flow as a criterion for the inception of liquid loading. These models assumes that, the film thickness is uniform in the pipe cross-section at all inclination angles. However, the gravitational

force acting on the liquid film causes the liquid film to become much thicker at the bottom than at the top. Their assumption of uniform film thickness results in under-predicting the critical gas velocity for inclined wells.

Luo et al. (2014) and Shekhar et al. (2017) made some improvements on the Barnea's model to include the variable film thickness for inclined wells and using different interfacial friction factors. Luo et al. (2014) model also included the Wallis (1969) droplet entrainment correlation. However, this correlation does not depend on liquid rate. It under-estimates the fraction of droplet entrainment for wells with higher liquid rate and also produce large errors for the fraction of entrainment greater than 0.5 (Berna et al. 2015). The Shekhar et al. (2017) model did not consider the effect of droplet entrainment. The results from Luo's model were still more conservative as compared to that of Shekhar.

In this thesis, further modifications have been made in the Luo et al. (2014) model by replacing the Wallis (1969) droplet entrainment correlation by the Oliemans et al. (1986) entrainment correlation. Similar entrainment correlation was also incorporated into the Shekhar et al. model. The results showed an improvement to the Shekhar et al model while the Luo's model still over-predicts the critical gas velocity. The outputs from different liquid loading criteria were also compared to quantify their accuracy with regard to the operating conditions of the well.

In addition to that, the evaluation of the Liquid loading criteria was done along the entire section of the wellbore to determine the loading status at every position in the tubing. It was suggested that the evaluation of critical gas velocity should be done at both the wellhead and the bottomhole.

1.1 Problem statement

Accumulation of liquids in gas wells is the most critical problem that hinders the productivity of gas wells. It causes reduction in the effective permeability around the wellbore and creates the back pressure against the formation. This in turn causes a rapid decline in gas production rate, reduction in the ultimate recovery of a gas well and if immediate unloading actions are not taken, the well may eventually die.

Several models have been developed to predict the inception of liquid loading in gas wells. However, each model outputs a different critical gas flow rate estimate. Some models under-estimates the critical gas velocity while other models over-estimates the critical gas velocity. Most

of the recent studies have concluded that the liquid loading in gas wells is caused by liquid film reversal rather than the droplet reversal as suggested by Turner et al. (1969).

The present work will therefore compare both the droplet model of Turner et al. (1969) and the liquid film reversal models of Barnea (1987,1989), Luo et al. (2014) and Shekhar et al. (2017) using the data available in the literatures. The effect of droplet entrainment in the film reversal models will be studied and based on the results, improvement will be suggested. This work will also explore the best evaluation point of the onset of liquid loading along the wellbore.

1.2 Objectives

The main objective of this master thesis is to compare some traditional and recent models used to predict liquid loading in gas wells and suggest for improvement based on the results. A secondary objective is to study the effect of the spatial variations of properties along the tubing when estimating the critical gas flow velocity.

1.3 Specific objectives

(i) To review selected existing traditional and recent models used to predict the inception liquid loading in gas wells.

(ii) To study the effect of droplet entrainment in the film reversal models by changing the amount of liquid transported on the wall (assuming the rest is entrained in the liquid core).

(iii) To study the effect of pressure and temperature variation along the tubing on the amount of liquid and gas velocity computed for each measured depth and on the liquid loading criteria.

1.4 Scope of the study

This work will be based on the review of some traditional and recent models used to predict the onset of liquid loading in gas wells. The liquid loading models of Turner et al (1989), Barnea (1986,1987), Luo et al. (2014) and Shekhar et al. (2017) will be studied followed by proposing and improving the liquid loading criteria of the liquid film reversal models by including the effect of droplet entrainment. The model will also explore the impact of variation in pressure and temperature along the tubing on the liquid and gas velocities at a given depth.

2.0 FUNDAMENTALS OF LIQUID LOADING IN GAS WELLS

2.1 Concept of liquid loading

Liquid loading is the accumulation of liquids at the bottom of the well during gas production when the available energy is insufficient to lift the co-produced liquids to the surface. This occurs when the velocity of the dominant phase (mainly gas) drops below a certain threshold known as critical velocity (Bolujo et al. 2017). When this velocity is reached, the gas starts to lose the ability to lift the produced liquids to the surface, therefore, liquid starts to collect at the bottom of the well.

The flow of gas and liquid along the tubing at high gas velocities cause the gas to drift towards the center of the tubing, creating a vortex known as a gas core. Liquid is forced out of the gas core to the walls of the tubing forming a liquid film. The shear force acting on gas-liquid film interface results to the formation of the liquid droplets that are transported in the gas core while some droplets are dropped back to the film forming the annular-mist flow pattern (Hernandez, 2017). High gas-liquid ratio under this flow pattern, results into lower pressure gradient in the tubing. Although the pressure loss due to friction increases with increase in gas velocity, its component is small and has little effect on the overall pressure drop in the tubing (Binli, 2009).

As the pressure in the reservoir declines, the gas velocity along the tubing also decreases with time. When the critical velocity is reached at the wellhead (position of the lowest velocity along the tubing), the liquid starts to accumulate at the bottom of the well. The liquid rate becomes greater than that of gas causing the hydrostatic pressure in the well to increase, this results to the increase in pressure gradient in the tubing. Continuous accumulation of liquids in the wellbore imposes an additional back pressure against the formation which lowers the gas production rate. Pressure in the reservoir then builds up, which pushes the accumulated liquids to the surface under intermittent or slug flow. Under this flow pattern, the liquid pockets separate the gas core. The cycle continues until the reservoir pressure build up is insufficient to push the liquids to the surface. At this point, the well will fail to produce gas and therefore it can be abandoned if some measures are not taken to unload the liquids (Luo et al. 2014).

2.2 Sources of liquids in the gas wells.

Production of liquids in gas wells may occur in almost every gas well at some point during the life of the well. Liquids entering the wellbore during gas production originate from multiple sources depending on the condition and type of the reservoir. Formation water is one of the most common

sources of water which is naturally trapped in the rock pores during the time of sedimentation. When gas flows into the well, this water can also flow to the well bottom along the fractures. Other sources of liquids include; water and hydrocarbon condensation, water coning, water production from a different zone, aquifer water, some external liquids introduced in the reservoir such as drilling fluids, fracturing fluids and any other fluid used in exploration and development (Zhang, et al. 2015). One or more of these sources of liquids may exist in the reservoir and the produced liquids have to be continuously transported to the surface for efficient operation of the well.

2.3 Gas-Liquid flow pattern

The geometrical distribution of gas and liquid flowing together in a conduit is governed by the dominant physical forces acting on a system and complex interfacial distribution factors such as surface tension, body forces, coalescence, dispersion, heat flux effects and wettability (Falcone et al. 2009). Depending on the magnitude of these forces, liquid and gas will form different flow patterns (flow regimes). The identification of flow patterns was traditionally done by visual scrutiny in transparent narrow tubes which yields accurate and reproducible results at moderate velocities. At high flow velocities, it is hard to see the distribution of the fluids in the tube, which makes the flow pattern identification difficult in various thermodynamic systems (Azzopardi, 2002). The most recent methods used to improve flow pattern recognition include the use of photographs with high speed flash, high speed video studies, analysis of spectral content of the unsteady pressures and volume fraction fluctuations.

The classification of flow patterns has been studied by various researchers who proposed numerous names and classification systems. However, for practical purpose, similar flow patterns are often grouped under the same name. The flow patterns differ depending on the size and orientation of the flow channel in which the fluids are flowing. Since the behavior and distribution of the flowing phases are slightly different for horizontal, vertical, and slopped pipes, it is therefore essential to describe the flow patterns separately for vertical and horizontal flow (Kumar, 2010).

2.3.1 Flow patterns for vertical pipes

Four basic flow patterns (regimes) usually occur in a vertical production conduit of a gas well with associated liquid are discussed. The flow patterns and their stage in the life of the well are as shown in **Fig. 2.1.**

Bubble flow - Under this flow regime, the flow channel is almost filled with liquid as a continuous phase while gas bubbles are suspended in the liquid as discrete substances. The pressure gradient along the tubing is determined by the liquid which is the continuous phase with some minor pressure drops caused by the presence of gas bubbles.

Slug flow **-** This flow pattern is also called plug flow when it occurs in horizontal systems. It is characterized by the presence of a series of liquid plugs (slugs) separated by relatively large gas pockets. It occurs when gas bubbles collide and coalesce to form bubbles of size approaching to that of the flow channel. The formed bubbles are bullet-shaped surrounded by thin films of liquid. They are commonly referred to as "Taylor bubbles". Two Taylor bubbles are separated by a liquid slug filled with smaller bubbles (Gao et al. 2014). Presence of high momentum liquid slugs induces forces especially at the point where the flow channel changes direction resulting into severe damage of the tubing. The flow regime also results in fluctuation of liquid and gas flow rate creating large pressure drop in the tubing which may completely kill the well (Fabre, 2015).

Churn flow **-** This is a distributed flow of gas and liquid characterized by the presence of very thick and unstable liquid films oscillating up and down with a net upward flow. The instability is caused by the gravity and shear forces acting in opposite direction on the thin liquid film surrounding Taylor bubbles. When the gas velocity rises, the bubbles breaks down leading to unstable pattern where churning of liquid occurs in the tubing, hence the name ***Churn flow*** arise. This type of flow regime only appears in vertical and near-vertical tubing. The flow regime is sometimes known as a ***transitional*** regime or ***semi-annular flow*** due to its complexity. Both the slug and churn flow patterns are also grouped as ***Intermittent flow*** since all causes high pressure drop and void fraction fluctuation in the tubing.

Annular/Mist flow - The flow is characterized by the liquid film flowing on the walls of the tubing, with the gas travelling at the center of the tubing forming a gas core. Also, some liquid droplets are entrained in the gas core. At high flow rates, most of the liquid are transported in gas core as droplets resulting into a ***mist flow***. However, in most cases the liquid will flow as film along the walls of the tubing except for very hot heat transfer systems that limits wetting. Under certain circumstances, the liquid flow rate may increase resulting to the increase in droplet concentration in the gas core of annular flow. This causes large lumps or streaks as wispy liquid occurring in gas

core (Kumar, 2010) resulting to another form of flow pattern called ***Wispy annular flow*** (Azzopardi, 2002)**.**

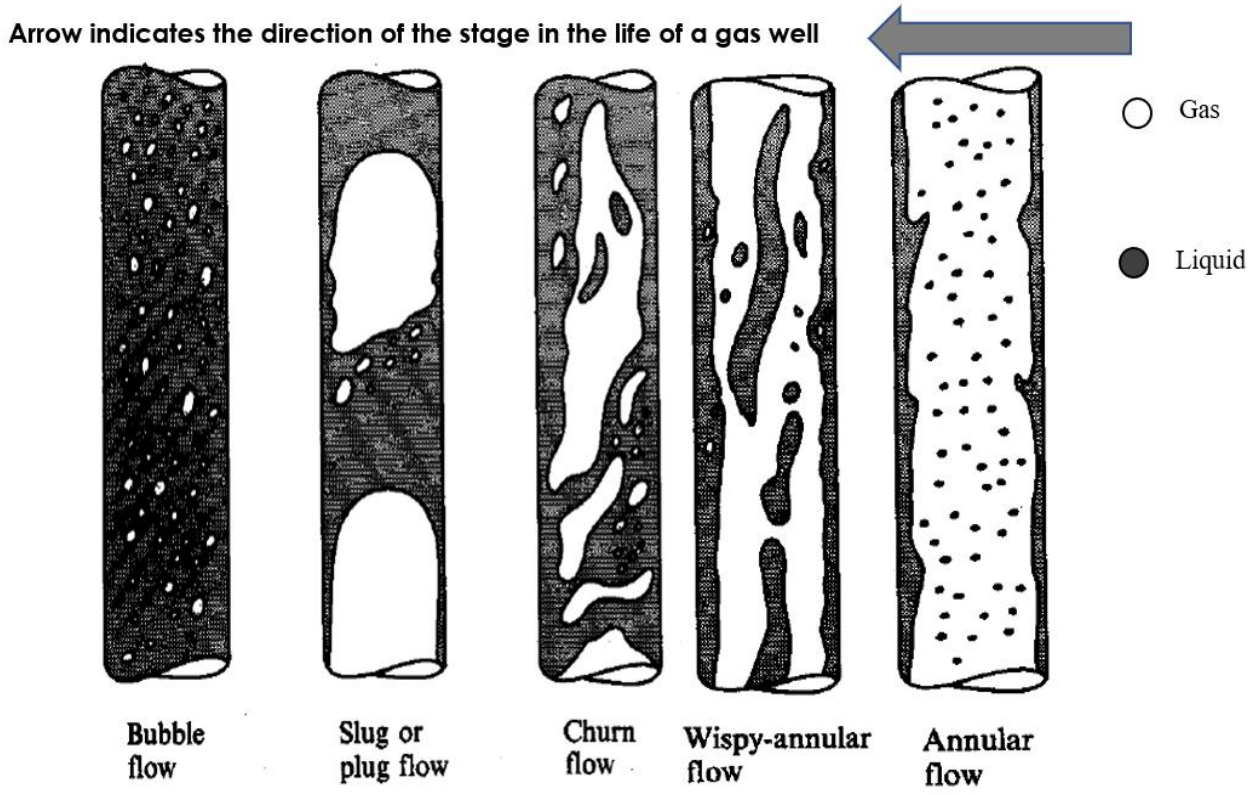

Fig. 2.1 - Two Phase flow pattern in a vertical pipe (Kumar, 2010).

2.3.2 Flow patterns for horizontal pipes.

This flow pattern is discussed here because when dealing with inclined system one gets flow patterns in between vertical-horizontal. The flow of gas-liquid mixture in a horizontal pipe is almost similar to that in the vertical pipe. The only difference is that, the distribution of the phases is affected by the gravity forces acting perpendicular to the tube axis. Gravity tends to stratify the heavier component (liquid) to the bottom and the lighter component (gas) to the top of the pipe. Depending on the gas-liquid ratio, superficial velocities and physical properties of the mixtures, the following are the most accepted classification of flow patterns for the horizontal pipe; These flow patterns and their configurations are shown in **Fig. 2.2.**

Stratified flow – The flow regime is gravity dominant whereas the liquid flows at the bottom of the pipe and gas at the top of the pipe with no significant waves at the gas-liquid interface. This occurs at low gas and liquid flow rate

Wavy flow – This flow pattern is similar to stratified but have significant interfacial waves. This occurs at high gas flow rates, where the interfacial shear stress at the gas-liquid interface increases causing the formation of waves that oscillates up and down along the interface, but usually the waves do not touch the top side of the pipe

Plug flow – Under this flow pattern, the bullet-shaped elongated gas bubbles are formed, and they tend to move at the top side of the pipe closer to the pipe walls.

Slug flow – Further increase in gas velocity causes the amplitude of the waves to grow and reach the upper walls of the pipe forming liquid slugs. These liquid slugs are carried by the fast-moving gas flow. The fast-moving series of liquid slugs are associated with sudden pressure pulses and oscillations that can damage the downstream components (Darzi & Park, 2017).

Annular flow – Under this flow pattern, the liquid forms a continuous phase along the walls of the pipe and the gas flows as vortex along the center of the pipe with some entrained liquid droplets.

Bubbly flow - The flow pattern exist at high liquid flow rate where the gas bubbles are relatively small compared to the liquid. The buoyancy force causes the gas bubbles to rise to the top of the pipe.

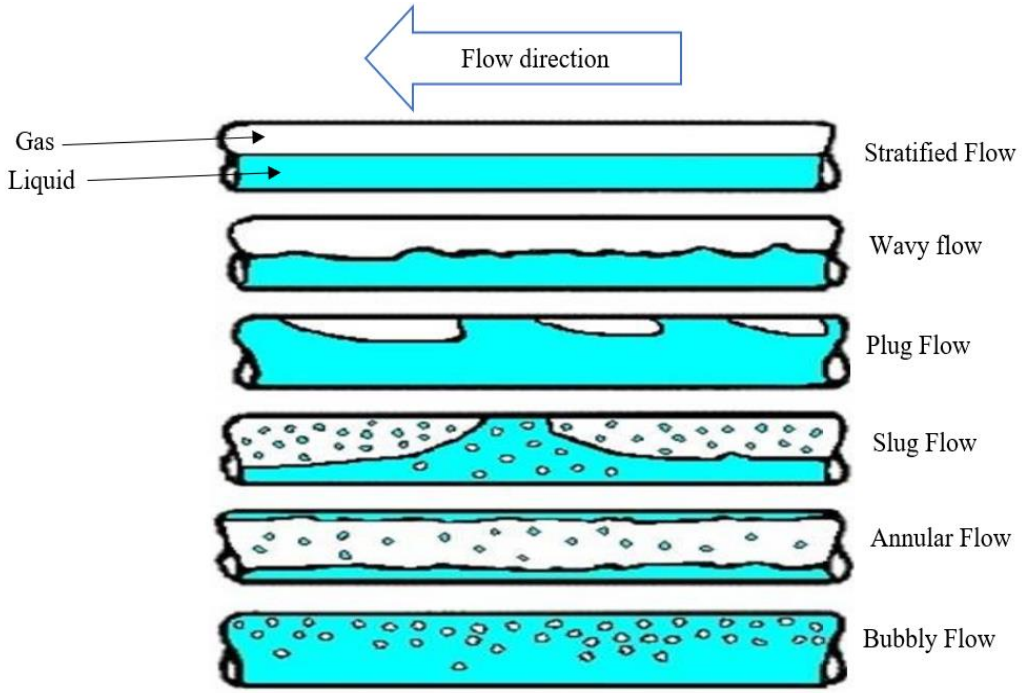

Fig. 2.2 - Flow regime of gas-liquid flow in a horizontal pipe (Darzi & Park, 2017)

2.3.3 Flow pattern for inclined pipes

For inclined pipe systems, the flow patterns depend on the angle of inclination from the vertical. For nearly vertical pipe systems, the flow patterns are relatively similar to that of vertical flow. Churn flow seldom occurs for pipes inclined above 20° from the vertical, while bubbly flow never occurs if the pipe is deviated for more than flow occurs 50° from the vertical. For near horizontal system, stratification starts to be observed (Perez, 2007).

2.4 Liquid loading models

Prediction of the inception of liquid loading in gas wells have been studied by several researchers. The studies are based on either development of new models or modification of the existing models for better prediction of the onset of liquid loading. Generally, liquid loading is described by two liquid transport mechanisms in gas wells; the liquid droplet reversal and the liquid film reversal. All the proposed models are based on one or all of these liquid transport mechanisms to predict the inception of liquid loading.

2.4.1 Liquid- droplet reversal model

The initial work on the critical rate required for continuous removal of liquids in gas wells was conducted by (Duggan, 1961) who observed that a linear velocity of 5ft/sec at the wellhead is sufficient to keep a gas well flowing under unloaded condition. His work was later extended to account for water-gas systems, where it was suggested that a velocity of 5 to 10ft/sec was adequate for hydrocarbon liquids removal and 10 to 20ft/sec was sufficient to lift the produced water (Koperna, 2004).

The entrained liquid-droplet model derived by Turner et al. (1969) is the most famous method for predicting the onset of liquid loading in gas wells. The model suggests that, liquid loading occurs due to falling back of liquid droplets in gas core. A droplet falling freely in a gas column is subjected to two forces; The Drag force from the gas (F_{drag}) acting upwards and a gravitational force due to the droplet weight (F_{weight}) acting downwards (Lea et al. 2011). The drag force and the force due to weight of the droplet are given in Eqn. (1) and Eqn. (2) respectively. The droplet will move upwards only if $F_{drag} > F_{weight}$ and downwards if $F_{drag} < F_{weight}$. When these two forces are equal, a terminal velocity is reached. A terminal velocity depends on the size, shape, and density of the particle in suspension, and the viscosity and density of the fluid medium (Coleman, et al. 1991).

$$F_{drag} = C_d \frac{\pi d^2}{4} \frac{\rho_g V_g^2}{2} \quad (1)$$

$$F_{weight} = (\rho_L - \rho_g) \frac{4}{3} \pi \left(\frac{d}{2}\right)^3 g \quad (2)$$

Where C_d is the drag coefficient, $\boldsymbol{d}$ [m] is the droplet diameter, ρ_g and ρ_L is the gas density and liquid density [kg/m^3], V_g is the gas velocity [m/s].

Turner et al. (1969) calculated a terminal velocity of the gas required to suspend a liquid droplet in gas stream by equating Eqn. (1) and Eqn. (2). The resulting terminal velocity $V_{g,T}$ [m/s] is as shown in Eqn. (3).

$$V_{g,T} = 3.617 \sqrt{\frac{d(\rho_L - \rho_g)}{C_d \rho_g}} \quad (3)$$

It can be observed that the terminal velocity in Eqn. (3) is directly proportional to the square root of the droplet diameter (d). Due to the turbulence nature of the flow in gas wells caused by high gas flow velocity, the droplets of different sizes in gas stream tend to coalesce and break up (Zhou & Yuan, 2010), while surface tension helps to hold the droplets together (Asheim, 2017). The turbulent force can be expressed in terms of friction force $\left(F_f = 0.5 f_d \rho V_g^2 A_d\right)$ and the force due surface tension is expressed in terms of interfacial tension and circumference of the droplet $(F_\sigma = \sigma S_d)$. To completely lift all the produced liquids out the well, the gas velocity should be able to lift the largest diameter liquid droplet. (Hinze, 1955) defined a Weber number as the ratio between the turbulent force and the force due to surface tension for the largest droplet diameter. For round droplets, the Weber number is presented in Eqn. (4). Where V_{gc} is the sinking velocity of the largest droplet.

$$We = \frac{\rho_g V_{gc}^2 d}{\sigma} \quad (4)$$

Different Experiments have revealed that, the critical value of Weber number for liquid falling freely ranges from 20-30 (Asheim, 2017). After considering this range, Turner et al. (1969) assumed that, the Weber number of 30 corresponds to the diameter of the largest droplet.

The drag coefficient is influenced by the shape of the droplet and its Reynolds number. For spherical droplets and turbulent region which is always the operating condition of gas wells, C_d is relatively constant with Reynolds number and stabilizes at 0.44. Substituting Eqn.(4) into Eqn.(3) under the conditions stated above, the Critical velocity is calculated as shown in Eqn.(5).

$$V_{sg-Critical} = 5.465 \frac{\left[\sigma(\rho_L - \rho_g)\right]^{1/4}}{\rho_g^{1/2}} \quad (5)$$

Where $V_{sg-critical}$ is the gas critical superficial velocity [m/s], σ, is the interfacial tension [N/m]. Similarly, in Eqn. (5), $V_{sg-Critical}$ can be computed in Field units by replacing the coefficient of the model (5.465) by 1.53 with σ [dynes/cm] while ρ_L and ρ_g in [lbm/ft^3]

The critical velocity Eq.(5) calculated by Turner et al. (1969) was tested against the field data and was found to match 66 out of the 90 tested wells. To improve the match of the field data, they added a 20% adjustment to the original equation to account for the Weber number which was established for air-water experiment instead of gas well condition (Kelkar et al. 2015) and the assumption of solid spheres to the drag coefficient instead of oscillating liquid droplets (Riza et al. 2016). Eqn.(6) gives the new critical velocity after 20% upward adjustment.

$$V_{sg-Critical} = 6.558 \frac{\left[\sigma(\rho_L - \rho_g)\right]^{1/4}}{\rho_g^{1/2}} \quad (6)$$

They tested Eqn.(6) against the field data and it was found to match 77 out of 90 tested wells. Turner et al, thus concluded that a 20% upward adjustment is necessary to improve the match of the well data. For computing $V_{sg-Critical}$ in field units a coefficient of the model in Eqn.(6) is replaced by 1.92 and all other inputs in field units.

Coleman et al.(1991) used the original Turner model to their well data and they found a reasonable match ,while Turner's adjusted model did not match their well data. Therefore, they concluded that a 20% upward adjustement is not necessary for low rate gas wells with wellhead pressures below 500 psia.

Nosseir et al. (2000) revealed that the reason why the Turner's model fails to predict some well data is because it neglects the occurance of different flow patterns in the well depending on the flow conditions. They suggested critical rate equations based on Transition flow regime and

assuming turbulent flow. They advised to take care of the existing flow conditions so that, relevant equation is applied for each flow regime when calculating critical flow rate. For wells having more than one flow regime, they recommended to carry out calculations at the wellhead pressures as it is a point of maximum gas slippage and hence maximum velocity which will ensure maximum critical flow rate required to keep gas wells unloaded.

Turner's model assumes a spherical shape of the droplet entrained in gas stream, however, under high gas velocity, a liquid drop deforms to ellipsoidal shape as shown in **Fig. 2.3** due to the pressure difference between the front and rear portion of the liquid drop. To account for the deformation of the entrained liquid droplet under high velocity gas, Li et al. (2001) deduced new model for calculating the critical velocity required for continuous unloading of gas wells. The model resulted into smaller critical velocity than that of the conventional Turner's model. However, the results were found to match fairly data obtained from gas wells in China gas fields.

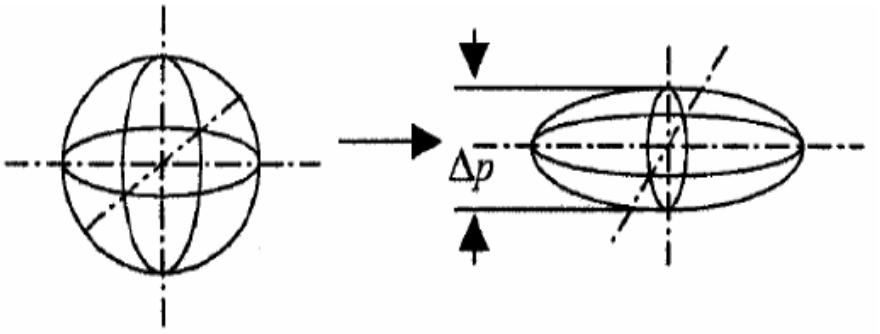

Fig. 2.3 - Shape of the liquid droplet in high gas velocity (Li, et al., 2001)

Turner's model does not account for the effect of well diameter and inclinations. It therefore gives inappropriate prediction for large diameter and inclined wells as discussed by (Kelkar & Sarica, 2015). Belfroid et al. (2008) modified the Turner's model to account for the effect of well inclination. They stated that the critical gas rate is lower for large inclinations from the vertical since the effect of gravity is reduced. Also, large inclination angles thicken the liquid film at the bottom of the tube cross section than at the top resulting to the increase in critical gas rate. The highest critical gas rate occurs at the medium range of inclination angle (about 30^o from the vertical). The critica superficial gas velocity in (m/s) propsed by Belfroid, et al. (2008) is given by;

$$V_{sg\ critical} = \left(3.1A\sqrt{\rho_g}\ \left[\sigma(\rho_L - \rho_g)\right]^{1/4}\right)\frac{(\sin(1.7\beta))^{0.38}}{0.74} \quad (7)$$

Where A is is the tube area [m^2] and β is the inclination angle [degrees]from the horizontal.

The multiphase air-water flow experiments conducted by Westende et al. (2007) to study the behavior of the droplet by measuring its size and velocity indicated that, liquid loading was not caused by the droplet reversal mechanisms but rather due to film reversal. This is because the droplet size used in the Turner's model is too large to exist under gas well conditions and therefore the Weber number may be below 30 (Westende, 2008). The Weber number used in Turner's model after 20% adjustment is 60, signifying that the droplet model may not be accurate for the prediction of the inception of liquid loading.

Veeken et al. (2010) examined the validity of Turner et al. (1969) model with their offshore data. They defined a Turner ratio as the ratio between the observed critical rate to the Turner critical rate. The ratio had a value in the range of 1.0 to 2.0 meaning that the Turner's model under-estimates the critical velocity. Therefore, they concluded that liquid-film reversal is the cause of liquid loading instead of the liquid-droplet reversal.

Turner et al, recommened to perform calculations of liquid loading conditions at surface (wellhead) conditions. This is convenient because the wellhead pressures and temperature data are easily available. However, Sutton et al. (2010) proposed that in some situations such as change in downhole geometry or when the tubing is set above perforations, the use of wellhead conditions as the evaluation point may result to erroneous conclusion. Hence, they stated that, when calculating critical velocity, wellhead conditions should be used for high pressure wells ($P_{wh} > 1000\ psia$) while bottomhole conditions should be used for low pressures wells ($P_{wh} < 100\ psia$). Also, for wells producing free water and wellhead pressure less than 1000 psia, bottomhole conditions should be used. After the analysis of velocity profile along the tubing, they accepted Turner et al. (1969) safety factor to ensure that the well is unloaded along the whole flow path. From their study, they also suggested the use of water properties for σ and ρ_L when calculating the critical velocity and when performing the estimation for other fluids. This provides a conservative estimate because the water density is higher than for hydrocarbon fluids.

2.4.2 Liquid-film reversal models

This is another physical mechanism that triggers liquid loading in gas wells. The liquid film reversal model was also studied by Turner et al. (1969). Their analysis were based on the velocity profile of the liquid film as it moves upwards inside a tube. The predictions from the film reversal model did not represent the loading condition as compared to that of the droplet model. Their analysis also showed no dependence of calculated minimum lift velocity on the gas-liquid ratio for the liquid production range of 1 to 100 bbl/MMcf which contradicts observations using the theoretical film model . Therefore, they concluded that, liquid transport mechanism is not controlled by liquid film movement. This conclusion is contrary to (Veeken et al. 2010; Westende et al. 2007; Belfroid, et al. 2008; Luo, 2013 and Shekhar et al. 2016) who concluded that, liquid loading results from liquid-film reversal rather than the liquid-droplet reversal.

The limitations of Turner's droplet model have triggered the studies on the Liquid film reversal models. The film models are based on the flow pattern transition as the criteria for the inception of liquid loading. Zhang et al. (2003a, 2003b) developed a unified hydrodynamic model which uses slug flow dynamics as a starting point to model flow pattern transition. This is because slug flow is always found at the centre of the flow pattern maps. It shares transition boundaries with all other flow patterns. They considered the entire film zone in **Fig. 2.4** as the control volume to construct the momentum and continuity equations for slug flow.

$$\frac{\rho_L(v_T - v_F)(v_S - v_F) - \rho_C(v_T - v_C)(v_S - v_C)}{l_f} - \frac{\tau_F S_F}{H_{LF}A} + \frac{\tau_C S_C}{(1 - H_{LF})A} + \tau_I S_I \left(\frac{1}{H_{LF}A} + \frac{1}{(1 - H_{LF})A}\right) - (\rho_L - \rho_C) g sin\theta = 0 \quad (8)$$

For transition from slug flow to annular or stratified flow, the length(l_F) becomes infinitely long, the momentum exchange term (first LHS term of Eqn. 8) becomes zero. The critical velocity from slug to annular flow can be calculated provided that continuity equation and correct closure relationships are provided.

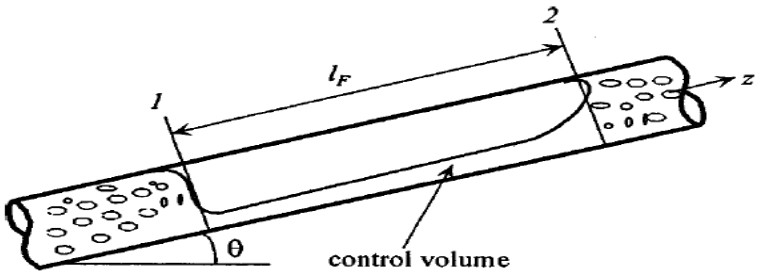

Fig. 2.4 - Control volume (Zhang, et al., 2003a)

Barnea (1986, 1987) proposed a unified model to analyze the transition from annular to slug flow. Under annular flow regime, the liquid film flows along the walls of the pipe and the gas flows at the centre as shown in **Fig. 2.5.** Transition from annular to slug flow occurs when the gas core is blocked by liquid lumps. There are two mechanisms which triggers the annular-slug transition; The first mechanism is the instability of the liquid film that restricts stable annular flow configurations, the second mechanism is the spontaneous blockage of gas core due to increased supply of liquid in the pipe. The most dominant cause of the inception of liquid loading is the liquid film instability since occurence of the second mechanism is associated with very high liquid flow rate which usually do not exist in most gas wells (Kelkar & Sarica, 2015).

2.4.2.1 Barnea (1986,1987) model

Modelling of the annular-slug transition was made on the basis of liquid film instability. To simplify the model, Barnea assumed that the film thicknes is uniform for all deviation angles of the pipe and the liquid flows as film along the pipe walls with no droplets entrained in gas core. The analysis of the liquid film interfacial shear change was done by constructing a momentum balance on both the liquid film and gas core separately as shown in Eqn. (9) and Eqn. (10) considering a steady state flow.

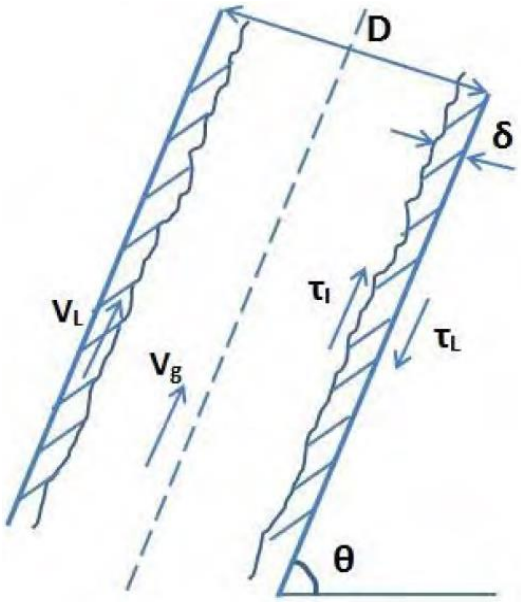

Fig. 2.5 - Liquid-gas annular flow in the wellbore (Kelkar, et al., 2015).

Momentum balance for the gas core

$$-A_G \frac{dP}{dZ} - \tau_I S_I - \rho_G A_G g Sin\theta = 0 \tag{9}$$

Momentum balance for the liquid film

$$-A_L \frac{dP}{dZ} - \tau_L S_L + \tau_I S_I - \rho_L A_L g Sin\theta = 0 \tag{10}$$

Eqn. (9) and Eqn. (10) can be combined to eliminate the pressure gradient. The combined momentum equation is as shown in Eqn. (11).

$$\tau_I S_I \left(\frac{1}{A_L} + \frac{1}{A_G}\right) - \tau_L \frac{S_L}{A_L} - (\rho_L - \rho_G) g sin\theta = 0 \tag{11}$$

The shear stress between the liquid and pipe walls is given by;

$$\tau_L = f_L \frac{\rho_L U_L^2}{2} \tag{12}$$

$$f_L = C_L \left(\frac{D_L U_L}{v_L}\right)^{-n} \tag{13}$$

$$D_L = \frac{4A_L}{S_L} \tag{14}$$

A_L, A_G, S_L, and S_I are dependent on the annular flow geometry and they are explained in detail

$$\tilde{\delta} = \frac{\delta}{D} \tag{15}$$

$$S_L = \pi D \tag{16}$$

$$S_I = \pi D\left(1 - 2\tilde{\delta}\right) \tag{17}$$

$$\mathrm{A_L} = \pi \mathrm{D}^2\left(\tilde{\delta} - \tilde{\delta}^2\right) \tag{18}$$

$$A_G = \pi D^2 \left(\frac{1}{2} - \tilde{\delta}\right)^2 \tag{19}$$

Where $\mathrm{A_L}$ and A_G are the cross-section area of the liquid and gas phase in the wellbore, respectively [m^2]; S_L and S_I are the liquid and interfacial circumferential length in the wellbore respectively

[m]; $\tilde{\delta}$ is the dimensionless film thickness [m], D is the pipe diameter [m], θ is the angle between the wellbore and the horizontal [°].

Substituting Eqn. (12) through (19) into Eqn. (11) and rearranging the combined momentum equation gives the expression for liquid-gas interfacial Shear Stress τ_I

$$\tau_I = g(\rho_L - \rho_G)DSin\theta\left(\tilde{\delta} - \tilde{\delta}^2\right)\left(1 - 2\tilde{\delta}\right) + \frac{1}{32}C_L\rho_L\left(\frac{\rho_L D}{\mu_L}\right)^{-n}(V_{LS})^{2-n}\left[\frac{\left(1 - 2\tilde{\delta}\right)}{\left(\tilde{\delta} - \tilde{\delta}^2\right)^2}\right] \qquad (20)$$

The interfacial shear stress provided by the gas phase is obtained from Wallis (1969) empirical equation as;

$$\tau_I = \frac{1}{2}f_I\rho_G\frac{V_{SG}^2}{\left(1 - 2\tilde{\delta}\right)^4} \qquad (21)$$

$$f_I = f_G\left(1 + 300\tilde{\delta}\right) \qquad (22)$$

$$f_G = C_G\left(\frac{V_{SG}\rho_G D}{\mu_G}\right)^{-m} \qquad (23)$$

$C_G = C_L$ = 0.046 for turbulent flow and $C_G = C_L$ = 16 for laminar flow

$m = n$ = 0.2 for turbulent flow and $m = n$ = 1 for laminar flow

In Eqn. (20), the interfacial shear stress (τ_I) is a function of liquid superficial velocity (V_{LS}) and Dimensionless film thickness ($\tilde{\delta}$). Solving for τ_I, requires V_{LS} and $\tilde{\delta}$ as inputs. The best idea is to plot the interfacial shear stress against the film thickness in dimensionless form ($\widetilde{\tau_I} = \tau_I/g(\rho_L - \rho_G)DSin\theta$ vs $\tilde{\delta}$) . This helps in detecting the annular- slug transition and the change in interfacial shear with liquid superficial velocity.

Table 2.1 - Barnea (1986,1987) test data for air water system

Inputs		
Item	**Units**	**Value**
Pressure	bar	1
Temperature	°C	25
Pipe Diameter	m	0.025
Gas Gravity (Air=1)	[ ]	1
Pipe Inclination (0 = Horizontal)	[°]	90
Liquid density	[kg/m^3]	1000
Gas density	[kg/m^3]	f(P, T)

For air water system with parameters presented in **Table 2.1**, a plot of $\tilde{\tau}_I$ against $\tilde{\delta}$ at different liquid superficial velocities, the series of curves shown in **Fig. 2.6** are obtained**.** The minimum point for each of the of curves corresponds to the point of transition from annular to intermittent/slug flow (Taitel et al. 1982). The solutions to the left of the transition point represents the annular (stable) flow while those to the right represents the slug (unstable) flow. The film thickness at the minimum point is the critical film thickness $(\tilde{\delta}_T)$. After obtaining τ_I and $\tilde{\delta}_T$ at the transition point, the gas superficial velocity can be calculated by substituting τ_I and $\tilde{\delta}_T$ in Eqn. (21). However, as the liquid flow rates increases the transition point is not observed, this means that the transition from annular to slug flow is not caused by liquid film instability any more, rather it occurs due to spontaneous blockage of gas core resulting from large supply of liquid.

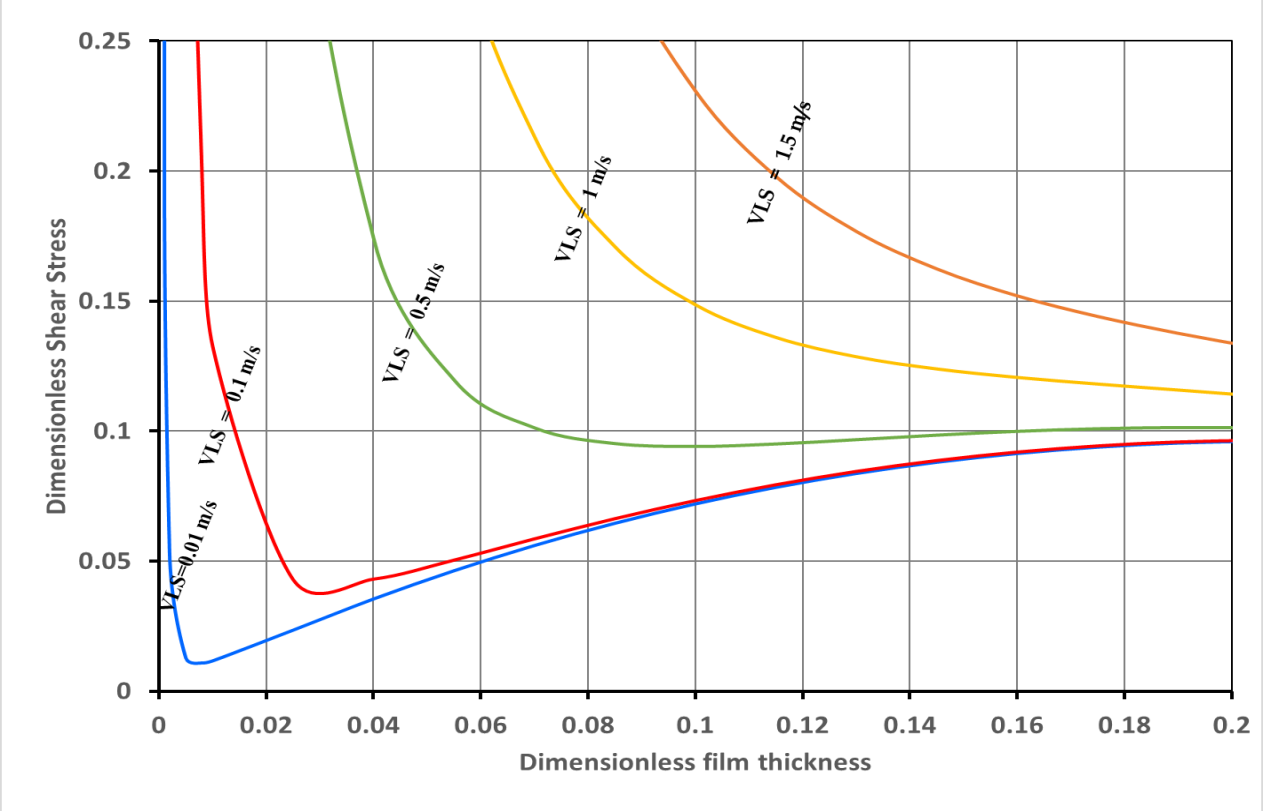

Fig. 2.6 - Variation of Interfacial shear stress with Liquid Film thickness at different liquid flow rates

The critical film thickness at the annular-slug flow transition point can also be obtained by differentiating Eqn. (20) with respect to $\tilde{\delta}$ and equating to 0, resulting to the following equation:

$$g(\rho_L-\rho_G)DSin\theta(\tilde{\delta}-\tilde{\delta}^2)(1-2\tilde{\delta})-\frac{1}{16}C_L\rho_L\left(\frac{\rho_L D}{\mu_L}\right)^{-n}(V_{LS})^{2-n}\left[\frac{(\tilde{\delta}-\tilde{\delta}^2)+(1-2\tilde{\delta})^2}{(\tilde{\delta}-\tilde{\delta}^2)^3}\right]=0 \qquad (24)$$

Using the data in **Table 2.1**, the solutions to Eqn. (24) at different liquid flow rates are as shown in **Fig. 2.7.** The point where curves crosses the x-axis ($d\tau/d\tilde{\delta} = 0$) represents the transition point from annular to slug flow. At lower liquid flow rates, the transition point exists, and each curve has two solutions. The leftmost solution corresponds to the critical film thickness at the transition point. The curves are observed to converge on the x-axis at a dimensionless film thickness of approximately $\tilde{\delta} = 0.14$. For large liquid rates, the curves do not cross the x-axis and therefore the solutions do not exist. This is an evidence to the fact that, the inception of liquid loading is not a result of liquid film instability rather, it is a result of spontaneous blockage of the gas core due to increased supply of liquids.

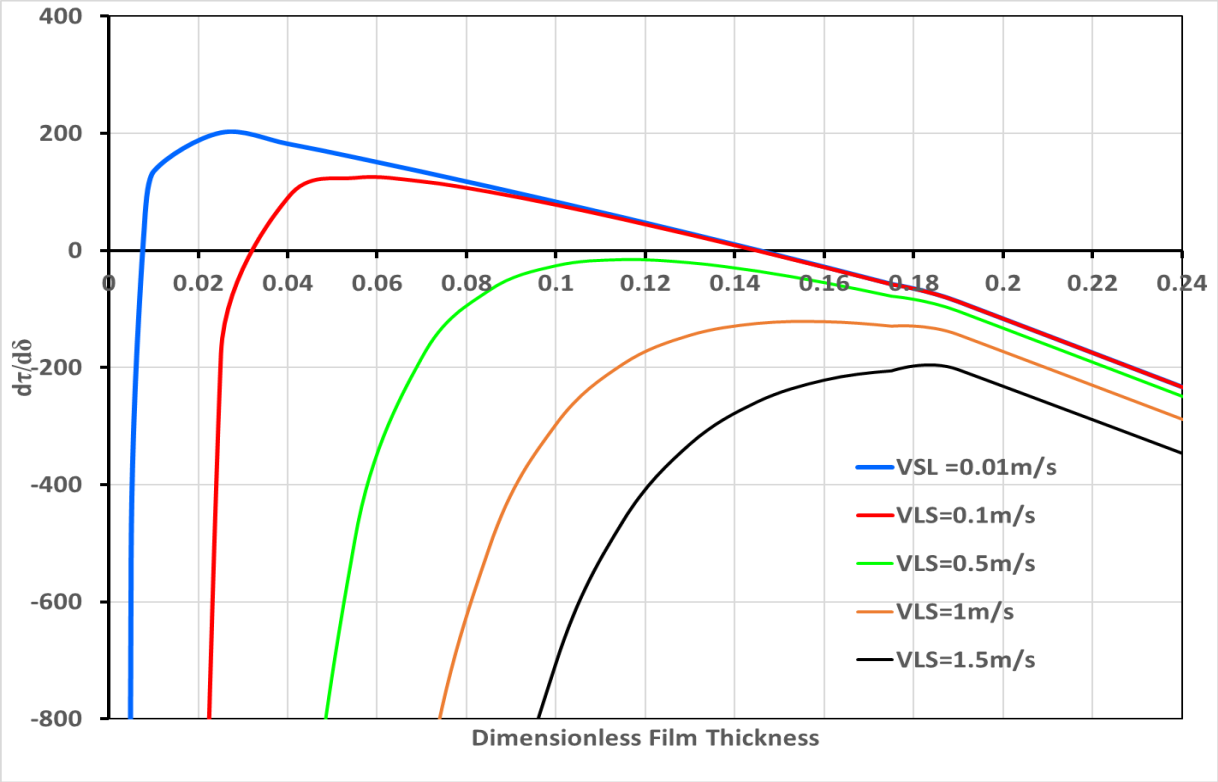

Fig. 2.7 - Solutions to critical film thickness at different Liquid superficial velocity

2.4.2.2 Luo et al. (2014) model

The accuracy of the Barnea's model in predicting the onset of liquid loading has been questionable due to its two considered simplifying assumptions. The first assumption is that the liquid exist as a film along the pipe with no droplet entrainment in the gas core. However, the turbulence nature of gas flow creates the shear force on the gas-liquid film interface resulting into the formation of the liquid droplets that are transported in the gas core (Thiruvengadam et al, 2009).

The second assumption is the use of uniform film thickness regardless of the deviation angle of the pipe. However, the deviation angle of the pipe has a greater influence on the liquid film thickness and therefore the resulting critical gas velocity. The air water experiment conducted by (Westende,2008) showed that the maximum critical velocity is observed when the deviation angle reaches 30º. There are two factors affecting the critical velocity for deviated wells; First, as the pipe deviates from the vertical, the film becomes thicker at the lower end of the pipe than at the top, requiring higher gas velocity to be transported to the surface. Second, the decrease in gravitational gradient as the pipe deviates. Since the gravitational gradient opposes the fluid flow, lower gravitation gradient reduces the critical gas velocity.

Since both gravitational gradient and thicker film exists as the pipe deviates, their combined effects determine the magnitude of critical velocity. **Fig. 2.8** shows that as the deviation angle changes from 0º to 30º the critical velocity increases, which means that the influence of thicker film thickness dominates the gravitational gradient and the overall effect results to higher critical velocity. As the deviation angle increases from 30º to 90º, the lower gravitational gradient dominates the thicker film thickness resulting to the reduction in critical gas velocity.

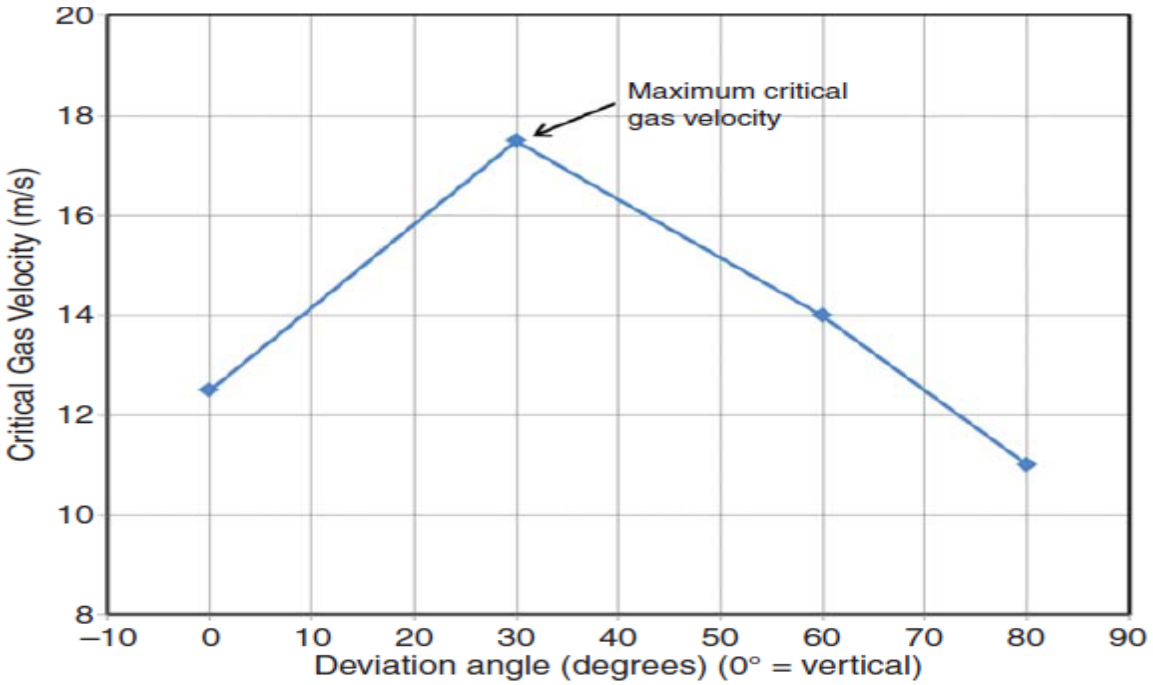

Fig. 2.8 - Critical gas velocity for different deviation angles of the pipe (Luo et al. 2014).

Luo et al. (2014) proposed a model to account for the limitations imposed by the Barnea's model. Three modifications were made as follows;

(i) Using the Fore et al. (2000) interfacial friction factor between the liquid film and the gas core instead of the Wallis (1969) correlation (Eqn. 22) used in the Barnea model which yields conservative results for the critical gas velocity. The new interfacial friction factor is;

$$f_I = 0.005\left\{1 + 300\left[\left(1 + \frac{17{,}500}{Re_G}\right)\frac{\delta}{D} - 0.0015\right]\right\} \tag{25}$$

(ii) Using a non-uniform film thickness for different deviation angles of the pipe. This was achieved by comparing a uniform and non-uniform film thickness models shown in **Fig. 2.9**. The comparison was made by using material balance to ensure that the mass flow rate of liquid transported in both cases is the same. For a uniform film thickness, the area of the uniform and non-uniform film thickness is given by;

$$A_1 = \pi D \delta_c \tag{26}$$

$$A_2 = \frac{1}{2}[\delta(0,\theta) + \delta(\pi,\theta)]\pi D \tag{27}$$

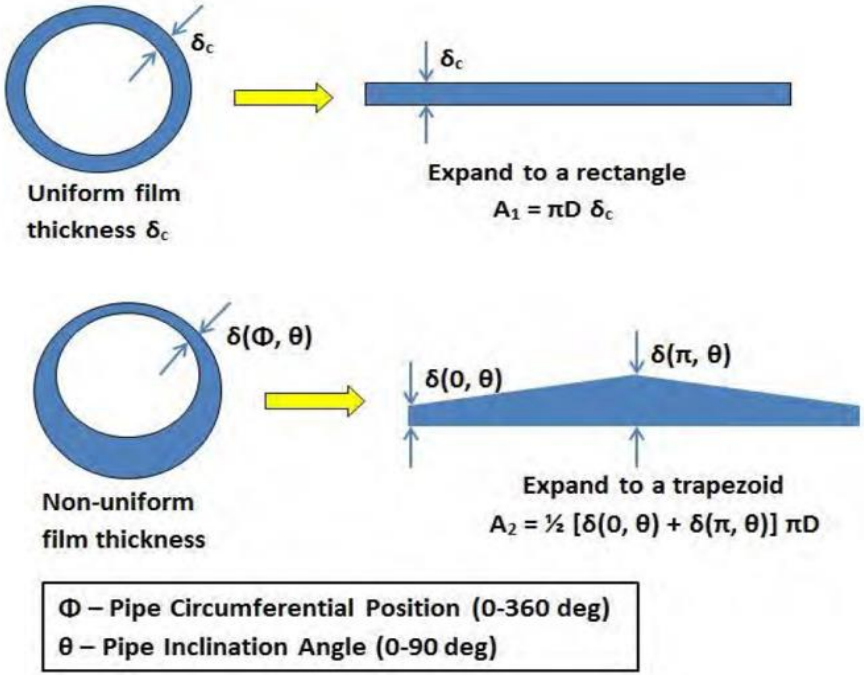

Fig. 2.9 - Schematic of uniform and non-uniform film thickness (Kelkar et al. 2015)

Since the mass flow-rate of liquid in both cases is conserved, Eqn. (26) and Eqn. (26) can be equated. The resulting relationship between uniform and non-uniform film thickness is;

$$\delta_c = \frac{1}{2}[\delta(0,\theta) + \delta(\pi,\theta)] \tag{28}$$

Where δ_c is the constant film thickness, D is the pipe diameter, $\delta(0,\theta)$ and $\delta(\pi,\theta)$ are the film thickness at the top and bottom of the pipe respectively. The film thickness distribution around the circumferential position of the pipe for different pipe deviation angles is shown in **Fig. 2.10** and can be obtained by using Eqn. (29) and Eqn. (30). The detailed description of these equations can be found in the paper by (Luo et al. 2014).

$$\delta(\Phi,\theta) = (1 - \alpha\theta cos\Phi)\delta_c \tag{29}$$

$$\alpha = \begin{cases} 0.0287, & 0 \le \theta < 30 \\ 0.55\theta^{-0.868}, & 30 \le \theta \le 90 \end{cases} \tag{30}$$

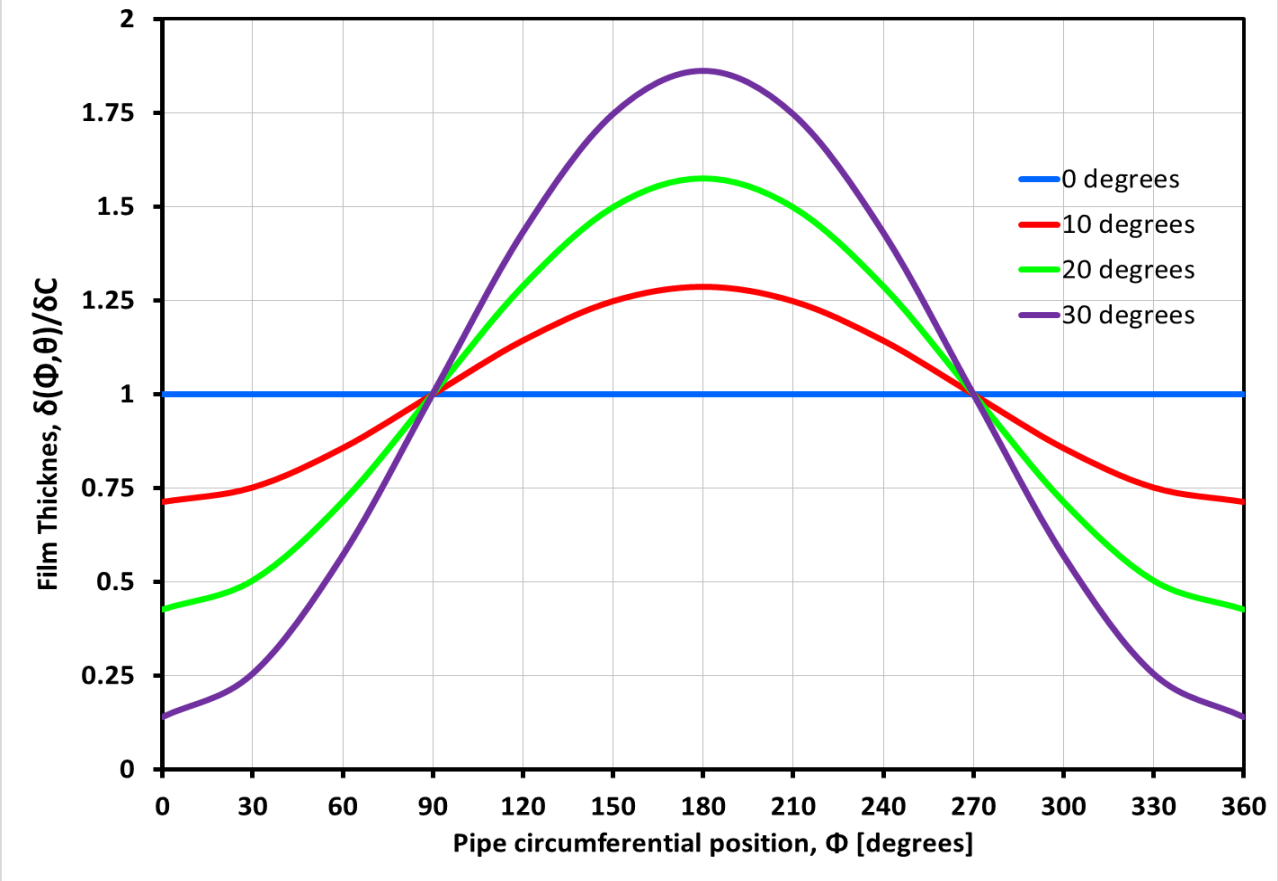

Fig. 2.10 - Film thickness distribution around the circumferential position of a pipe for different pipe deviation angles.

To incorporate the Luo et al. (2014) model of variable film thickness in the Barnea (1986,1987), first, the critical film thickness δ_T is calculated from Eqn. (24). This is the film thickness at the pipe bottom and represents the maximum film thickness at the transition point

which will initiate liquid loading. For calculating the critical velocity in deviated wells, δ_T is converted to δ_c by using Eqn. (29) where $\delta(\Phi,\theta)$=δ_T.

(iii) Including the droplet entrainment in the gas core. This was achieved by calculating the fraction of droplets entrained in the gas core (f_E) using the correlation proposed by Wallis (1969) as follows;

$$f_E = 1 - e^{[-0.125(\varphi - 1.5)]} \tag{31}$$

$$\varphi = 10^4 \frac{V_{SG}\mu_G}{\sigma}\left(\frac{\rho_G}{\rho_L}\right)^{0.5} \tag{32}$$

The liquid flow rate in the film can be calculated as;

$$q_F = q_l(1 - f_E) \tag{33}$$

2.4.2.3 Shekhar et al. (2017) model

Shekhar et al. (2017) modified the Barnea's model. They retained some findings from the Luo et al. (2014) model that the film thickness changes with the variation in deviation angle of the pipe. However, instead of calculating a constant film thickness (δ_c), as done by Luo, they calculated an average dimensionless film thickness ($\tilde{\delta}_{avgL}$) as;

$$\tilde{\delta}_{avgL} = \frac{1}{2}\left(1 + e^{-0.088\theta}\right)\tilde{\delta}_{max} \tag{34}$$

Where $\tilde{\delta}_{max} = \delta_T$ is the maximum or critical film thickness obtained by differentiating the combined momentum equation, and θ is the deviation angle of the pipe. For details of how Eqn(34) was derived, the reader is reffered to the paper by (Shekhar et al. 2017).

In addition to the variable film thickness, they revised the Wallis (1969) Liquid-gas interfacial friction factor. They proposed a correlation that is dependent on the deviation angle of the pipe as shown in Eqn (35)

$$f_i = f_{sg}\left\{1 + \left[340(1 + cos\theta)\tilde{\delta}_{avgL}\right]\right\} \tag{35}$$

They assumed the value of $f_{sg} = 0.005$ which represents the interfacial friction factor between the gas phase and the pipe wall in the absence of liquid phase. However as the pipe is inclined, a portion of the pipe is exposed to gas and the remaining portion is exposed to liquid with the

smallest value observed when the pipe is completely horizontal ($\theta = 90°$). The main difference between the (Luo et al. 2014) and (Shekhar et al. 2017) is on the use of different interfacial friction factors, different correlations for calculating the maximum film thickness to account the the change inclination angles of the pipe and neglecting the effect of droplets entrainment in the Shekhar et al model . The results obtained from (Shekhar et al. 2017) were optimistic (lower than those predicted by Barnea) as compared that of (Luo et al. 2014) which were conservative (higher than those predicted by Barnea).

3.0 PRESSURE DROP CALCULATION IN WET GAS WELLS

Prediction of pressure drop in pipelines is important in gas wells with or without some liquid production. It allows accurate projection of the achievable production rate, detection of scaling along the tubing, production optimization of surface facilities, design of artificial lift installations and design of cost effective well completions. Pressure measurement can be done using pressure gauges placed at a point of interest in the wellbore or with permanent bottom-hole gauges. However, performing these measurements is usually time-consuming and costly.

Several correlations have been proposed for prediction of pressure traverse along the wellbore. Some of these correlations were developed based on energy balance between two points (Poettman & Carpenter, 1952; Hagedorn & Brown, 1965) , some were derived based on the pressure balance (Duns & Ros, 1963) and others based on mechanical energy balance between two points in the system under consideration. However, the general form of equation for pressure gradient in flow strings is based on Bernoulli's equation neglecting the work done by the system. The equation is given by;

$$\frac{dP}{dL} = \frac{g}{g_c}\rho sin\theta + \frac{\rho v}{g_c}\frac{dv}{dL} + \frac{f\rho v^2}{2g_c d} \tag{36}$$

Where dP is the pressure loss due to elevation ($\frac{g}{g_c}\rho sin\theta$), acceleration ($\frac{\rho v}{g_c}\frac{dv}{dL}$) and friction ($\frac{f\rho v^2}{2g_c d}$) at a given interval dL, g is the acceleration due to gravity, g_c is the gravitational conversion constant, ρ is the fluid density, v is the fluid velocity, f is the friction factor and d is the diameter of a conduit.

3.1 Single phase gas wells

For dry gas, the pressure traverse in the tubing is calculated by using various methods such as; The average temperature and compressibility method by (Katz et al. 1959), The original Cullender and Smith method (Cullender et al, 1956), the modified Cullender and Smith method (Oden et al, 1988) and the Sukker and Cornell method (Guo et al, 2005) . However, the most common method is the simplified method by (Katz et al.1959). The method assumes that the temperature and compressibility factor are constant and are represented by the average values over the portion of the the tubing length considered. For single phase gas flow, it is also possible to assume that the change in kinetic energy is small and the pressure loss due to acceleration may be neglected.The equation is given by;

$$q_{gsc} = 200\left[\frac{SD^5(P_{in}^2 - e^s P_{out}^2)}{\gamma_g f_m \bar{Z}\bar{T} L cos\theta (e^S - 1)}\right]^{0.5} \tag{37}$$

$$S = 0.0375\frac{\gamma_g L cos\theta}{\bar{Z}\, R\, \bar{T}} \tag{38}$$

Where q_{gsc} is the gas flow rate in [Mscf/D], $\bar{Z}$ is the average gas compressibility factor [-], $\bar{T}$ is the average temperature [°R], γ_g is the gas specific gravity [-], D is the tubing diameter [in.], L is the measured depth [ft], θ is the inclination angle of the tubing from the vertical [°], P_{in} is the tubing upstream pressure [psia] and P_{out} is the tubing downstream pressure [psia]. The mood friction factor is a function of Reynolds number for a given tubing diameter and wall roughness of a pipe. For fully turbulent flow, which is the most common flow regime in gas wells, the friction factor can be expressed in terms of tubing diameter (Guo et al. 2005).

$$f_m = \frac{0.0175}{D^{0.224}} \quad for\ D \leq 4.277\ in \tag{39}$$

$$f_m = \frac{0.01603}{D^{0.164}} \quad for\ D > 4.277\ in \tag{40}$$

3.2 Multiphase gas wells

Prediction of pressure drop in wells producing under multiphase flow differs from those in single phase flow due to the complex nature of two phase flow. The previous mentioned correlations in subsection 3.1 are only valid for dry gas wells and wells with producing gas/liquid ratio (GLR) above 10,000 Scf/STB (Beggs, 1984). For wells with lower GLR, there is an additional pressure

loss due to slippage between the phases. This slippage causes the difference in the average linear velocity of the phases involved (Hagedorn & Brown, 1965).

Several correlations have been proposed to calculate the pressure drop in multiphase flow for vertical, inclined and horizontal wells. Some traditional models assumed that, liquid-gas flow in the conduit is homogeneous, this assumption ignores the effect of slippage caused by lower gas density that tends to overtake the liquid phase. However, in reality the flow of liquid-gas mixture is heterogeneous with different average linear velocity resulting from slippage.

Execution of the multiphase flow equations for pressure traverse calculations involves an iterative trial-and-error solution to account for the change in flow parameters as a function of pressure and temperature along the flow string. In the absence of computer programs, the calculation procedures are intensive especially when the flow string is discretized into several segments. There are two alternatives for which a pressure traverse calculation can be performed. The first alternative is by fixing pressure drop and finding the wellbore length interval for which the fixed pressure drop would occur. The second alternative is to fix the interval of the wellbore length and find the corresponding pressure drop in that interval. All these alternatives involves iterative procedures until convergence is achieved.

If a computer or computational routine is not available, pressure traverse curves can be used as an alternative solution for estimation of pressure as a function of depth. These curves are made from two-phase flow regime correlations for different gas-liquid ratios. However, a particular pressure traverse curve is limited to a given calculation procedure and flow situation, tubing size, liquid rate and water fractions.

Some of the multiphase flow correlations which are available for pressure drop calculations in wells and pipelines includes the (Duns & Ros, 1963), (Fancher & Brown, 1963), (Hagedorn & Brown, 1965), (Orkiszewski, 1967), (Beggs & Brill, 1973), (Gray, 1978), (Mukherjee & Brill , 1985) etc. For the purpose of this thesis, only (Gray, 1978) and the (Beggs & Brill, 1973) correlations are explained in detail.

3.2.1 Gray correlation

Gray (1978) developed a correlation for computation of pressure profile in gas condensate wells of vertical configurations. It uses the velocity number, nominal diameter, and the non-slip holdup

dimensionless variables to calculate the liquid holdup in the pipe. He observed that, liquid holdup in the well is mostly affected by the change in pipe wall roughness rather than the change in friction factor. The pressure loss is a result of the hydrostatic head and the frictional head loss, Eqn. (41). It gives accurate results for gas wells with condensate ratios up to 50 bbl/MMscf and high produced water ratios. The detailed description of Eqn. (41) is shown in **Appendix A.**

$$\frac{dp}{dz} = \frac{g\rho_m}{144g_c} + \frac{2f_{tp}{V_m}^2\rho_{ns}}{144g_cD} \tag{41}$$

3.2.2 Beggs and Brill correlation

Beggs and Brill (1973) published a correlation for predicting pressure drop and liquid holdup for multiphase flow. The correlation was developed for horizontal pipe and it was extended so that it can be applied for inclined pipes. The correlation often checks for the flow regime that would occur if the pipe were horizontal and then the holdup correction is made for other pipe inclinations. The inclination correction coefficients are different for different flow patterns. The detailed procedures for pressure traversing using the Beggs and Brill correlation is described in **Appendix B**. The equation has been observed to overpredicts pressure drop in vertical and inclined pipes.

4.0 RESULTS AND DISCUSSION

4.1 Comparison of the liquid loading models against field data.

In this section, the critical gas rate predicted from the liquid droplet model of Turner et al. (1969) and the liquid film reversal models of Barnea (1986,1987), Luo et al. (2104) and Shekhar et al. (2017) are compared and validated against selected field data. Three sets of well data published in the papers by Turner et al. (1969), Coleman et al. (1991) and Vakeen et al. (2010) are used. For each of these field data, the critical gas rate (q_{crit}) for each well was calculated and compared with the current (observed) gas rate (q_{actual}) in the field. A comparison of the model prediction against the field data was done by plotting q_{actual} against q_{crit} from the model predictions. The results are as follows.

4.1.1 Turner et al. (1969) Data

Turner et al. (1969) reported 106 vertical gas wells with liquid production. The wells were regarded as vertical since no inclination was reported in their data. The liquid loading status shows that 37 wells were loaded up, 53 wells were unloaded, and 16 wells were questionable. Comparison of the models was done using a total of 90 wells neglecting the wells reported as questionable. The liquid produced from the wells is either water or condensate and some wells produce both water and condensate. By using each of the aforesaid models, the critical gas velocity was calculated for each well by using relevant liquid properties of the liquid flowing in the well. If the well produces both water and condensate, the heavier liquid phase (water) properties were used in calculating the critical gas rate for both considered models. The typical fluid properties and conditions suggested by Turner et al. are shown in **Table 4.1.**

Table 4.1 - Liquid properties proposed by Turner.

Property	**Value**	**Units**
Gas gravity	0.6	-
Temperature	120	°F
Z-factor	0.9	-
Water density	67	lbm/ft^3
Water surface tension	60	dynes/cm
Condensate density	45	lbm/ft^3
Condensate surface tension	20	dynes/cm

The liquid loading models of Turner et al. (1969), Barnea (1986,1987), Luo et al. (2014) and Shekhar et al. (2017) were programmed to compute the critical gas superficial velocity, the resulting critical velocity was then converted to critical gas flow rates at standard conditions (14.7 psia and 60 ^{o}F) using Eqn. (42) in consistent units for a given pipe cross-section area (A) and gas volume factor (B_g). It was assumed that water and condensates are in liquid phase neglecting water vaporization and gas condensation. At high reservoir pressure and temperature, some liquid water can be in vapor phase. Also, the reduction in pressure and temperature along the tubing would cause condensation of some heavier hydrocarbon components into liquid phase. Therefore, the assumption that water and condensate are in liquid phase may lead to some errors since there might be less or more liquid in along the tubing.

$$q_{\bar{g}} = \frac{V_{sg}A}{B_g} \tag{42}$$

$$B_g = \frac{P_{sc}ZT}{PT_{sc}} \tag{43}$$

To construe the accuracy of model predictions, the actual gas flow rate was compared to the gas flow rate from the model predictions. If $q_{actual} > q_{crit}$, the well is unloaded, and if $q_{actual} < q_{crit}$, the well is loaded up. For precise predictions of the models, all the wells with unloading test status are expected to fall above a 45^{o} line and all the wells with loading test status are expected to fall below a 45^{o} line.

By applying Turner's model with the 20% upward adjustment suggested in their paper, the results are shown in **Fig. 4.1**. A comparison of q_{actual} against q_{crit} from Turner's prediction show that all 53 wells which were reported as unloaded were accurately predicted by the Turner's model with an accuracy of 100% while only 19 out of 37 loading wells were accurately predicted by the Turner's model with an accuracy of 51%. These observations signifies that, Turner's model can better predict the liquid loading condition for unloaded gas wells. On the other hand, the model underestimates the critical flow rate for wells producing under loaded condition.

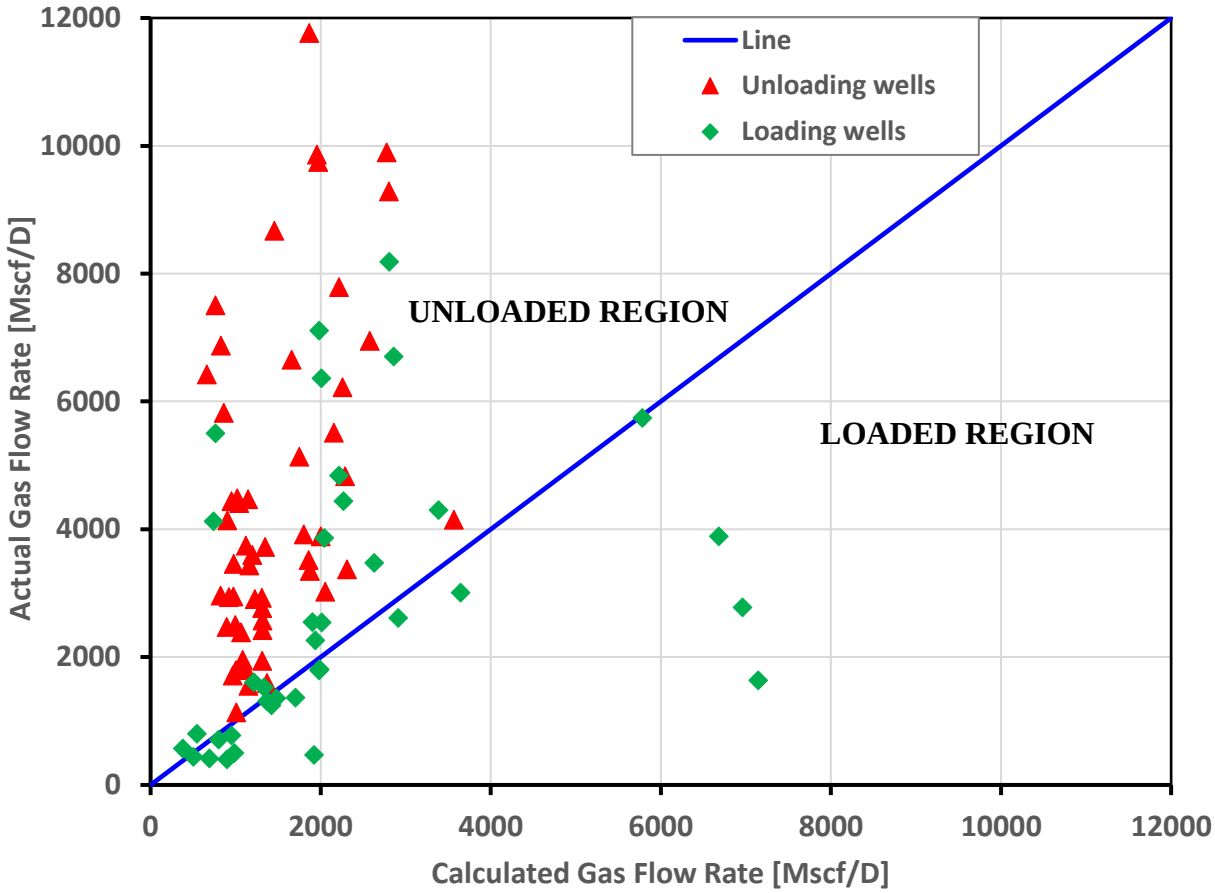

Fig. 4.1- Comparison of Actual gas flow rate vs Gas rate prediction using the liquid droplet model of Turner's et al (1969).

Turner's well data were also used to validate the liquid reversal model of Barnea (1986,1987) as shown in **Fig. 4.2**. The observed gas flow rates were compared to the critical gas flow rate predicted from Barnea's model. It was observed that, 39 out of 53 unloading wells were accurately predicted by the Barnea's model with an accuracy of 74% while 30 out of 37 loading wells were accurately predicted by the Barnea's model with an accuracy of 81%. This indicates that Barnea's model overpredicts the unloading wells by 26% and underpredicts the loading wells by 19%. From these observations, the overall consequence is that, the predictions of critical gas velocity from Barnea's model are conservative (over-estimates the critical velocity).

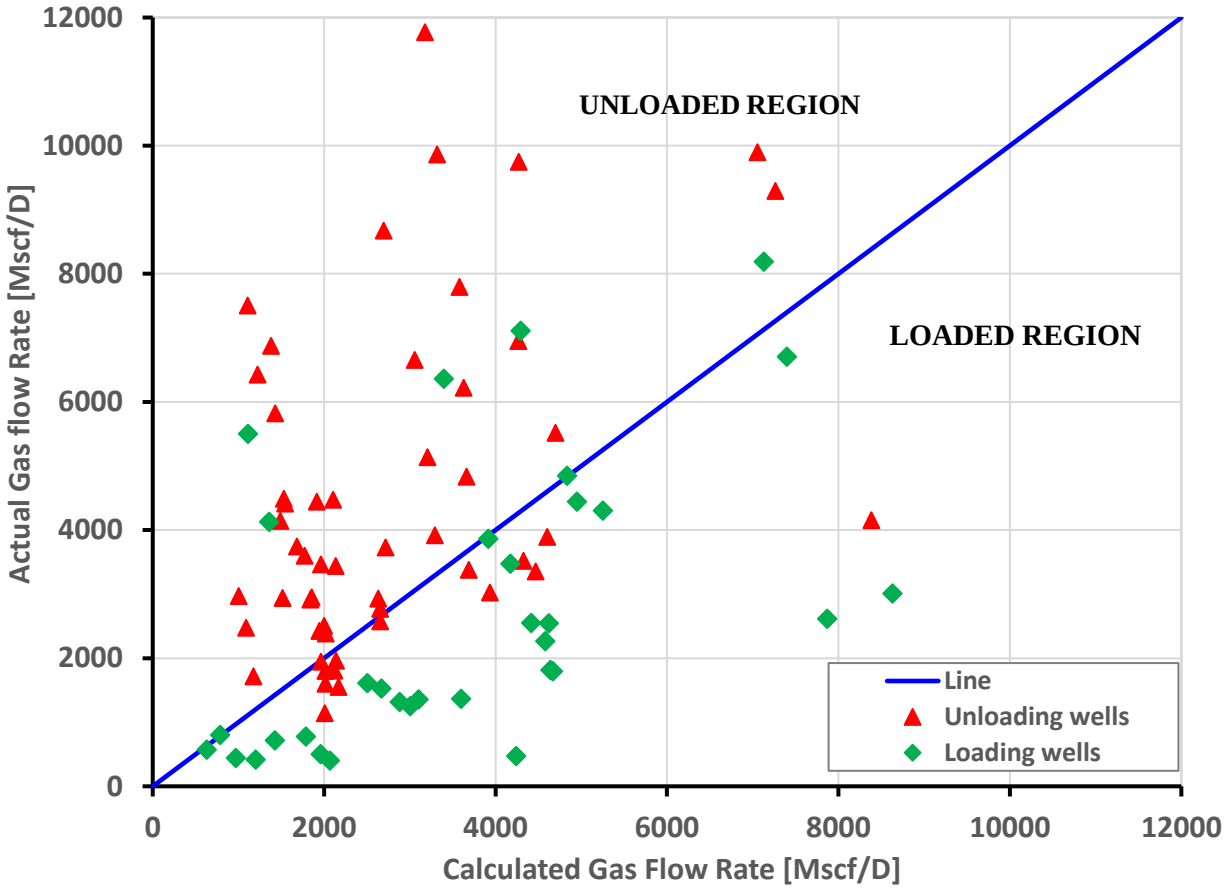

Fig. 4.2 - Comparison of Actual gas flow rate vs Gas rate prediction using Barnea's model

In **Fig. 4.3**, a comparison of q_{actual} against the q_{crit} predicted from the liquid film reversal model of Luo et al. (2014) was made. It was observed that, 46 out of 53 unloading wells were accurately predicted by the model with an accuracy of 87% while 26 out of 37 loading were accurately predicted by the model with an accuracy of 70%. The overall consequence is that the Luo's model over-predicts the critical velocity.

In **Fig. 4.4,** the predictions from Shekhar et al (2017) model shows that, 52 out of 53 unloading wells were accurately predicted by the model with an accuracy of 98% while 20 out 37 loading wells were accurately predicted by the model with an accuracy of 54%. This is also a good indication that the Shekhar et al (2017) can predict with greater accuracy the loading condition of gas condensate wells producing under unloaded conditions while it can also over-estimate the critical rate wells producing under loaded conditions.

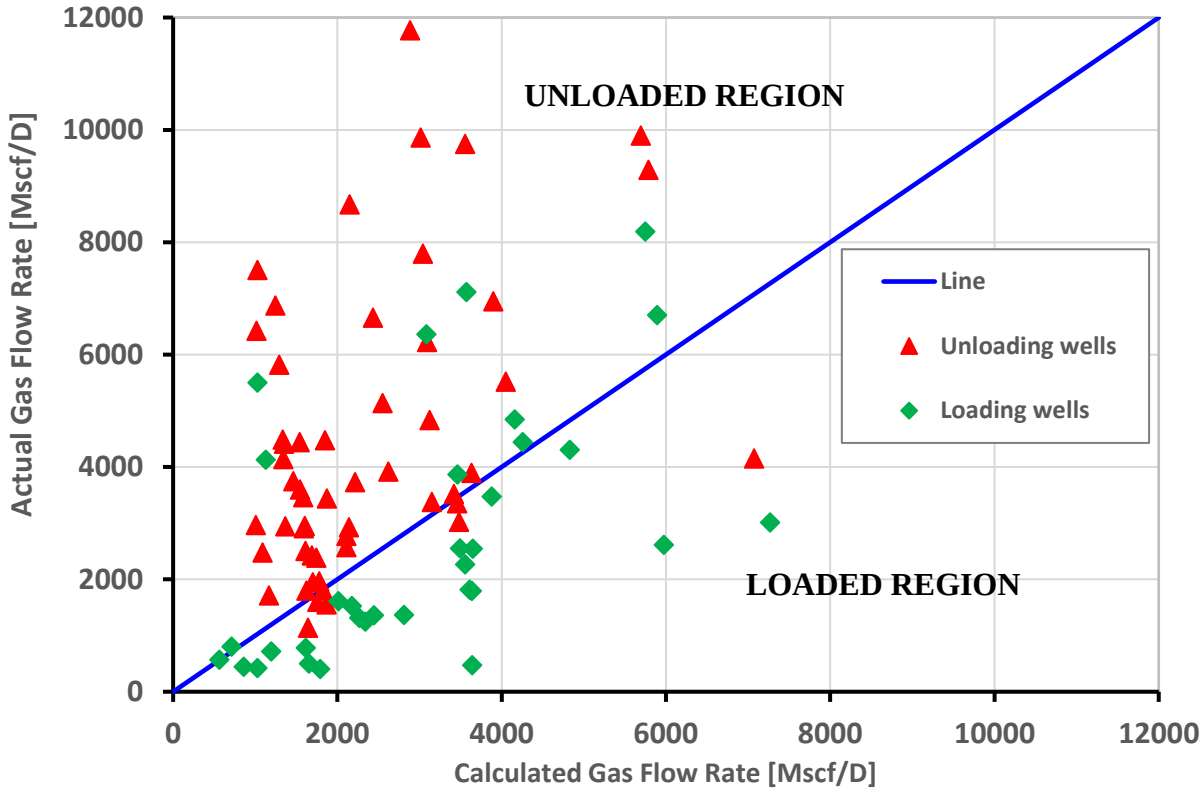

Fig. 4.3-Comparison of actual gas flow rate vs gas rate prediction using Luo et al. (2014) model

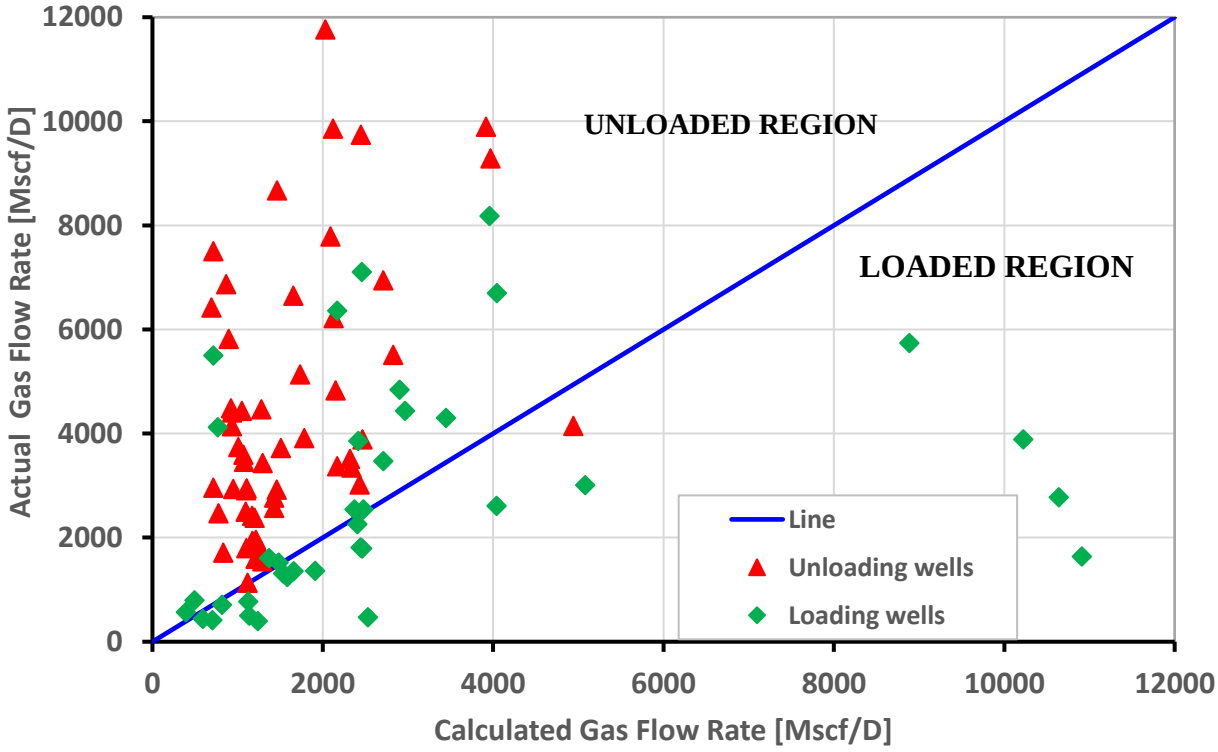

Fig. 4.4 - Comparison of actual gas flow rate vs gas rate prediction using Shekhar et al. (2014) model

The percentage accuracy of each of the considered models for predicting the onset of liquid loading is shown in **Fig. 4.5**. Using Turner's data, it was observed that, the liquid droplet model of Turner et al (1969) and the Liquid film reversal models of Shekhar et al (2017) can predict the status of unloaded wells with greater accuracy compared to other models under consideration. However, these models were observed to be inferior in predicting the onset of liquid loading in wells producing under loaded condition. The loading wells can be predicted with reasonable accuracy using Barnea's model which have shown accuracy up to 81% followed by Luo et al (2014) with an accuracy of 74%.

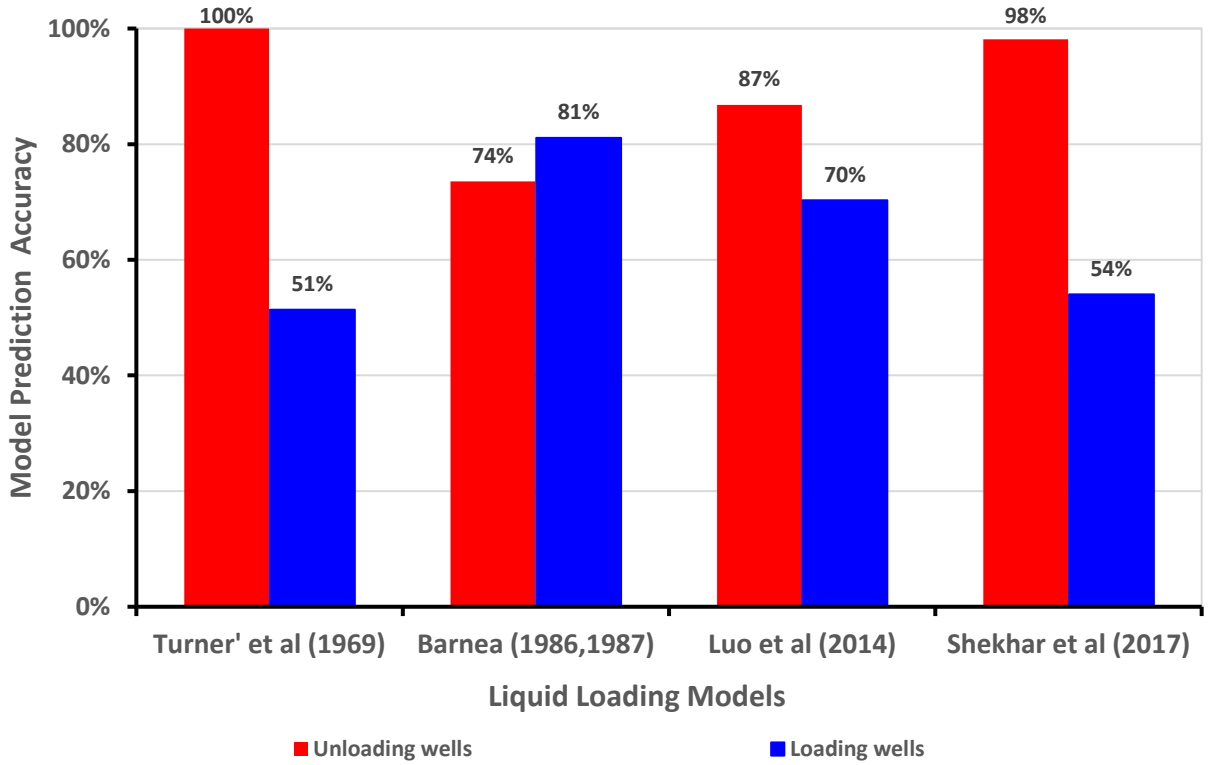

Fig. 4.5 - Critical Gas flow rate prediction accuracy from the Liquid loading models using Turner et al (1969) data.

4.1.2 Coleman et al. (1991) Data.

Coleman et al. (1991) published data from 56 gas wells with low wellhead pressure below 500 psia producing both water and condensate. They also reported the minimum gas flow rate required to initiate liquid loading in gas wells. This was achieved by adjusting the wellhead pressure to force all the wells to loading condition. The reported minimum flow rate is different from the Turner's actual flow rate who reported the current gas rate and the loading status of the well. Therefore, for accurate prediction of critical gas rate from the considered liquid loading models,

the plot of q_{actual} against q_{crit} from the model predictions should fall at, or slightly below the 45° boundary line separating the loaded and the unloaded region.

Since the reported wells produce both water and condensate, the model predictions were accomplished considering that the heavier liquid phase (water) as the primary source of liquid accumulation in the well. The basis of this assumption was verified by (Sutton et al. 2010) who stated that, equilibrium water vapor from the reservoir is always produced in all gas wells. These water vapor condenses out of gas in the tubing as the pressure and temperature decreases from the bottom of the well to the surface. The resulting critical gas rate from the droplet model of Turner and the considered liquid film reversal models of Barnea, Luo and Shekhar were compared to the actual gas rate as shown in **Fig. 4.6.**

The model comparison against the well data reported by Coleman et al. (1991) shows that the liquid droplet reversal model of Turner et al. (1969) without a 20% adjustment as proposed by Coleman et al. (1991) could better predict the loading condition of vertical wells with wellhead pressure below 500 *psia* as compared to the liquid film reversal models. For the Turner's model, most of the data points are observed to fall slightly below or above the 45° line which is a good indication of best fit of the data points to the boundary line separating the loading and unloading region. The liquid film reversal models did not show a best match to the actual well data with the Barnea's model being the worst in comparison to the Luo's and Shekhar's models.

To assess the accuracy of the model against the field data, the Root mean square error (RMSE) was calculated for each model using **Eqn. (44)**. RMSE is used as a measure of accuracy for which a perfect fit is achieved when its value is equal to 0 (never achieved in practice). The lower the RMSE, the greater the accuracy of the model prediction. RMSE was used instead of the percentage accuracy used in the Turner's data because of the difference in the reported actual gas flow rates. The minimum flow rate reported in the Coleman's data requires the gas rate predictions from the liquid loading models to fit in the 45° line, while the current gas rate and the loading status reported in the Turner's data requires the predictions to fall either above a 45° line for unloading wells or below the line a 45° line for loading wells. The results are as shown in **Fig. 4.7.**

$$RMSE = 100\%\, x \sqrt{\frac{1}{n}\sum_{i=1}^{n}\left(\frac{q_{observed} - q_{calculated}}{q_{observed}}\right)^2} \qquad (44)$$

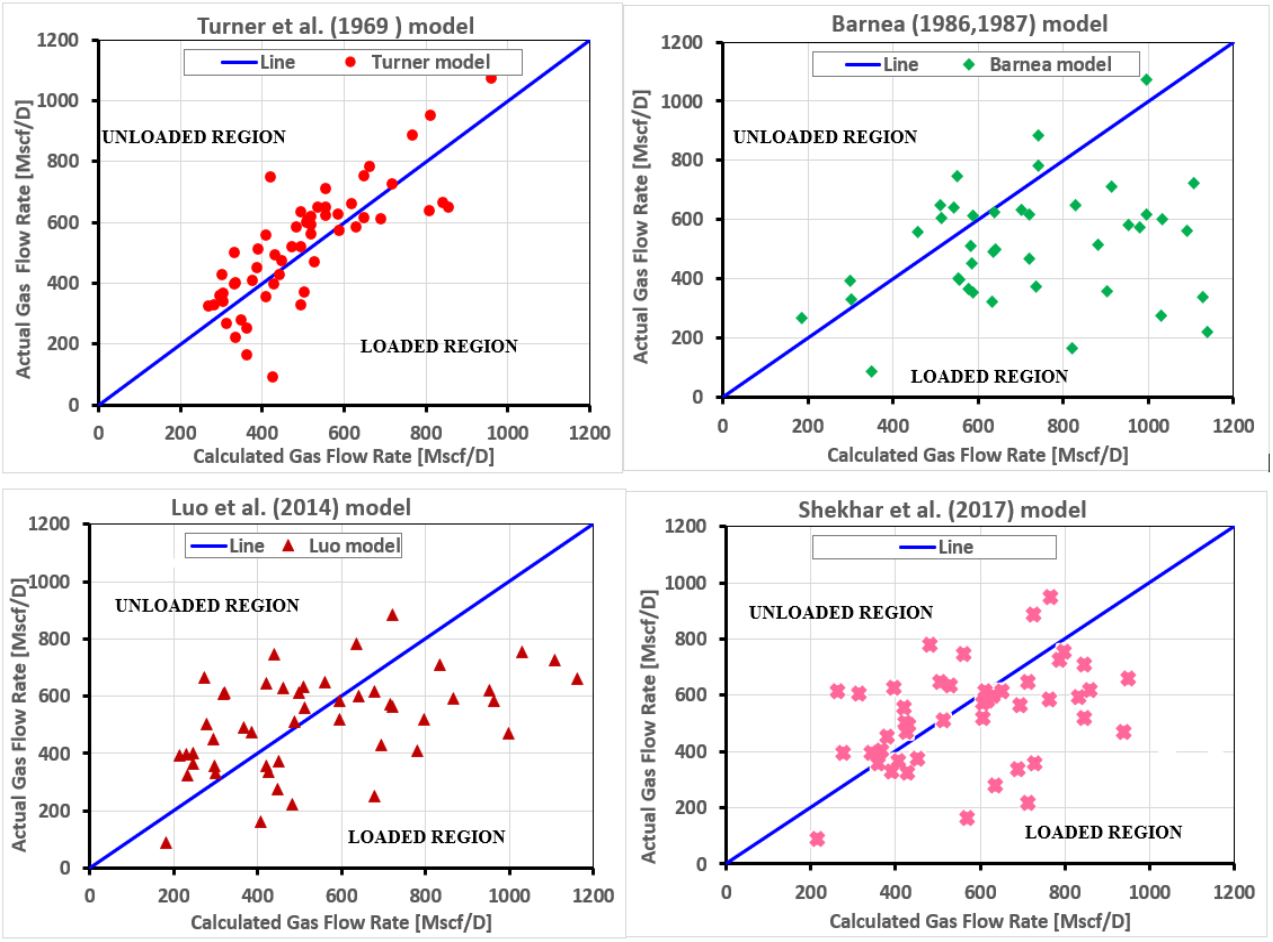

Fig. 4.6 - Comparison of critical flow rate predicted using Liquid loading model of Turner et al (1969), Barnea et al (1986,1987), Luo et al (2014) and Shekhar et al (2017) using Coleman's data set.

It can be clearly observed from **Fig. 4.7** that the prediction from Turner's model has lower RMSE as compared to the liquid film reversal models. This is an indication that the droplet model of Turner et al. (1969) can still be used to predict the onset of liquid loading with reasonable accuracy than the film reversal models for vertical wells with wellhead pressure below 500 psia, though the deviation from the actual well data is significant. By Comparing the Liquid film reversal models, the prediction from Barnea's model is the worst of all film models having the RMSE of 170 which is greater than all the compared liquid film reversal models while the predictions from the Luo's model shows better accuracy compared to all considered film reversal models.

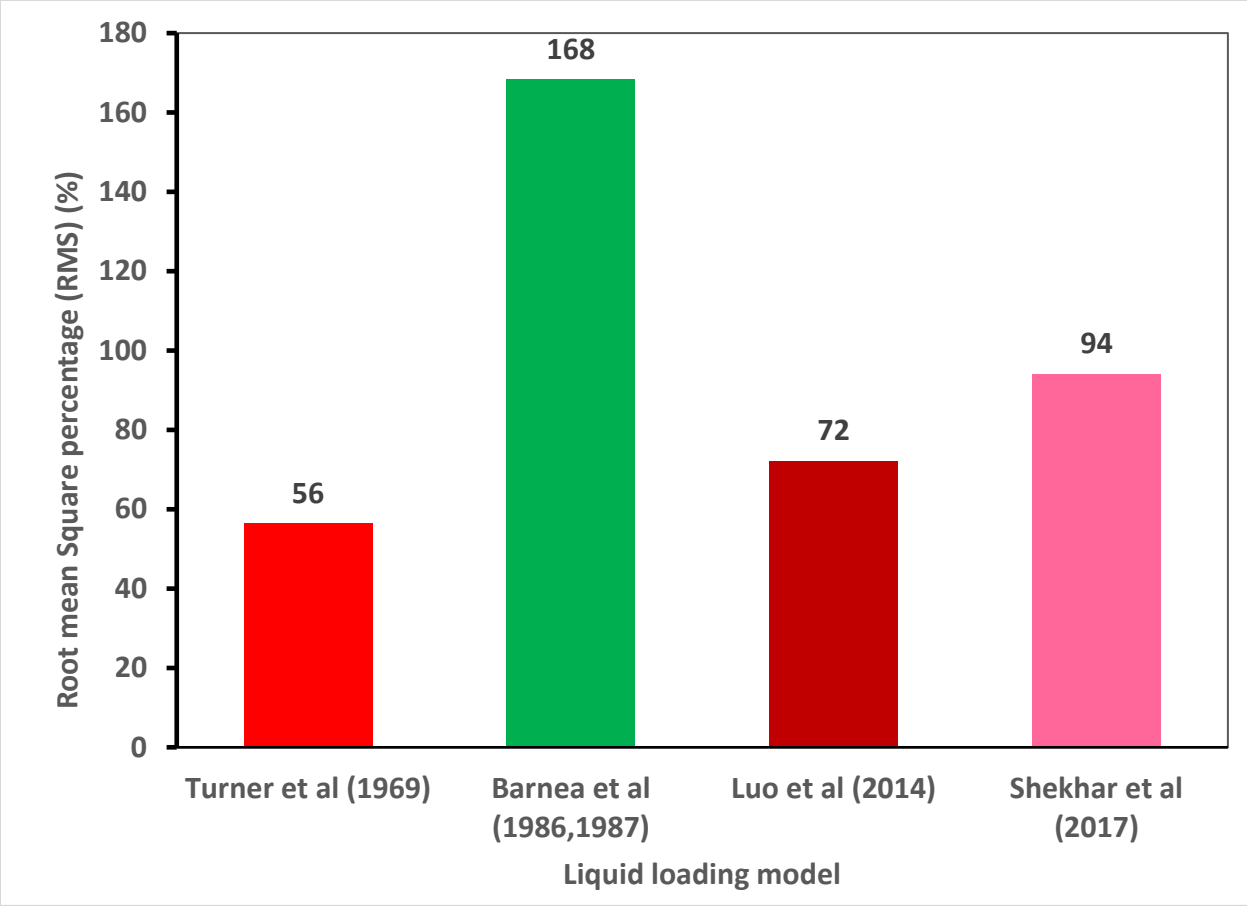

Fig. 4.7- Comparison of model accuracy in predicting liquid loading using Coleman et al (1991) data.

4.1.3 Veeken et al. (2010) Data

Veeken et al. (2010) reported a total of 67 gas wells from the offshore North sea . Their wells have large tubing size in the range of 2 to 6 inches and the inclination angle in the range of 0 to 64° from the vertical. The wells produce both water and condensate and most of the produced liquid comes from condensation of water. Similar to Coleman's data, they reported the minimum gas flow rate below which the wells will be producing under loaded condition. That means the critical gas rate prediction from the models should fall at, or slightly below or above the 45° line in the plot of q_{actual} against q_{crit} . Their data has no information concerning the daily liquid production, therefore a constant liquid production of 5bbl/MMcf was assumed.

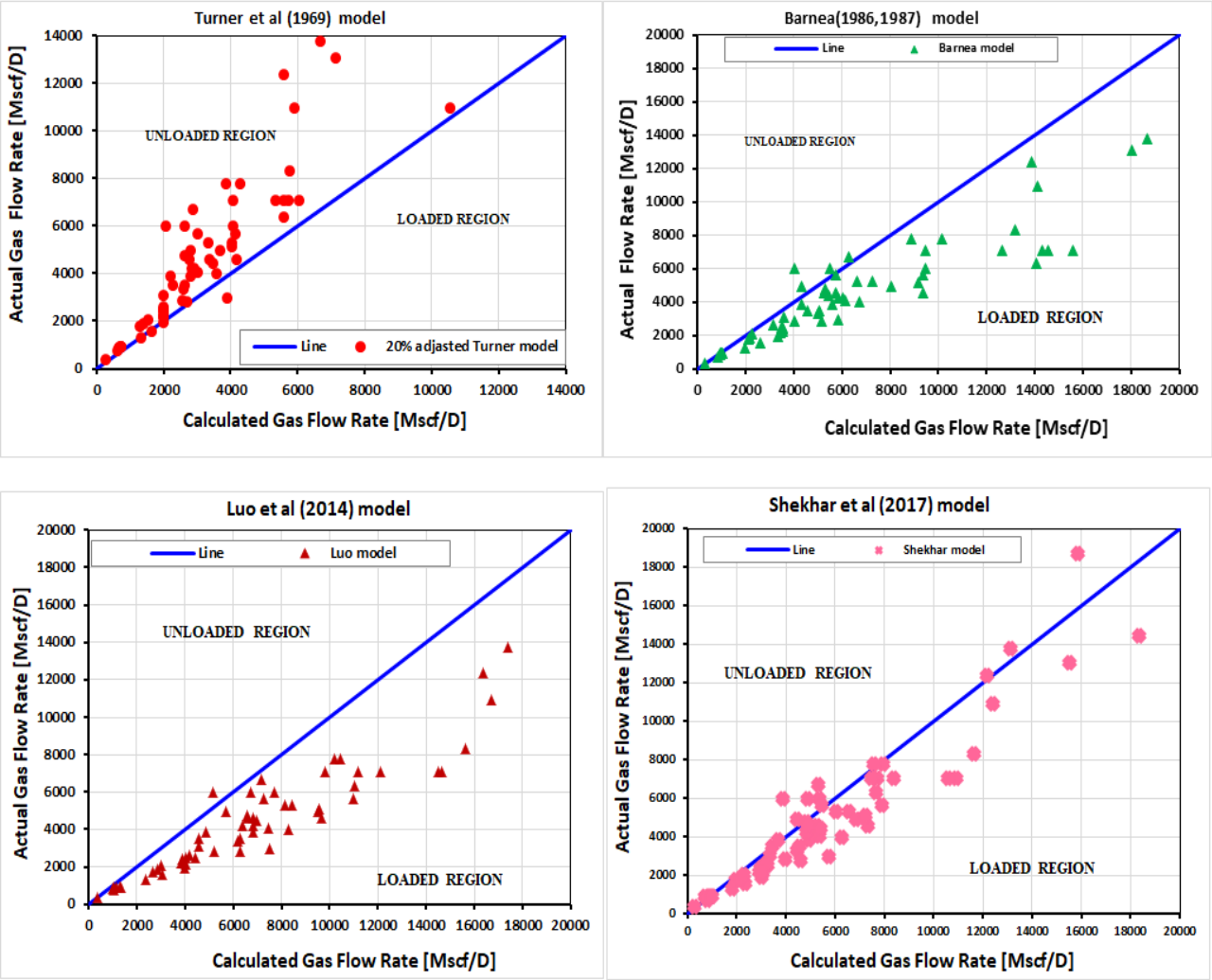

Fig. 4.8 - Actual gas rate vs Calculated gas Flow rate for different models using Veeken et al (2010) data.

The comparison of the model prediction against the actual field data using Veeken et al. (2010) data shown in **Fig. 4.8** indicates that the liquid film reversal model of Shekhar et al. (2017) was observed to predict most of the wells to be producing under loaded condition but slightly closer to boundary line separating the loading and unloading region (45° line). The predictions from the liquid droplet reversal model of Turner et al. (1969) were also observed to predict most of the wells to be producing under unloaded condition as the points fall slightly above the 45° line. The film reversal models of Barnea (1986,1987) and Luo et al. (2014) were observed to predict that the wells are producing under loaded conditions but most of the wells were observed to fall away from the 45° line. Since the accuracy of the model prediction increases as the points fall closer to the 45° line, then the model prediction far from the boundary line is an indication of the model failure to predict the critical velocity.

In order to identify the most accurate model out of the models compared, the RMSE was computed for each model as shown in **Fig. 4.9** . The film reversal model of Shekhar et al. (2017) was observed to be superior in predicting the onset of liquid loading with the RMSE of 33% which is lower than all the models under comparison. The predictions from Turner's model follows after the Shekhar model with the RMSE of 42%. Both the film reversal model of Luo and Barnea were observed to be conservative with the Luo's model having the highest RMSE of 71% as compared to that of Barnea's model which have the RMSE of 56%. Their predictions shows that the wells are loaded and most of the points fall away from the boundary line. Based on these observations, the Shekhar et al. (2017) model can better predict the onset of liquid loading for deviated wells with larger diameter in the range of 2 to 6 inches.

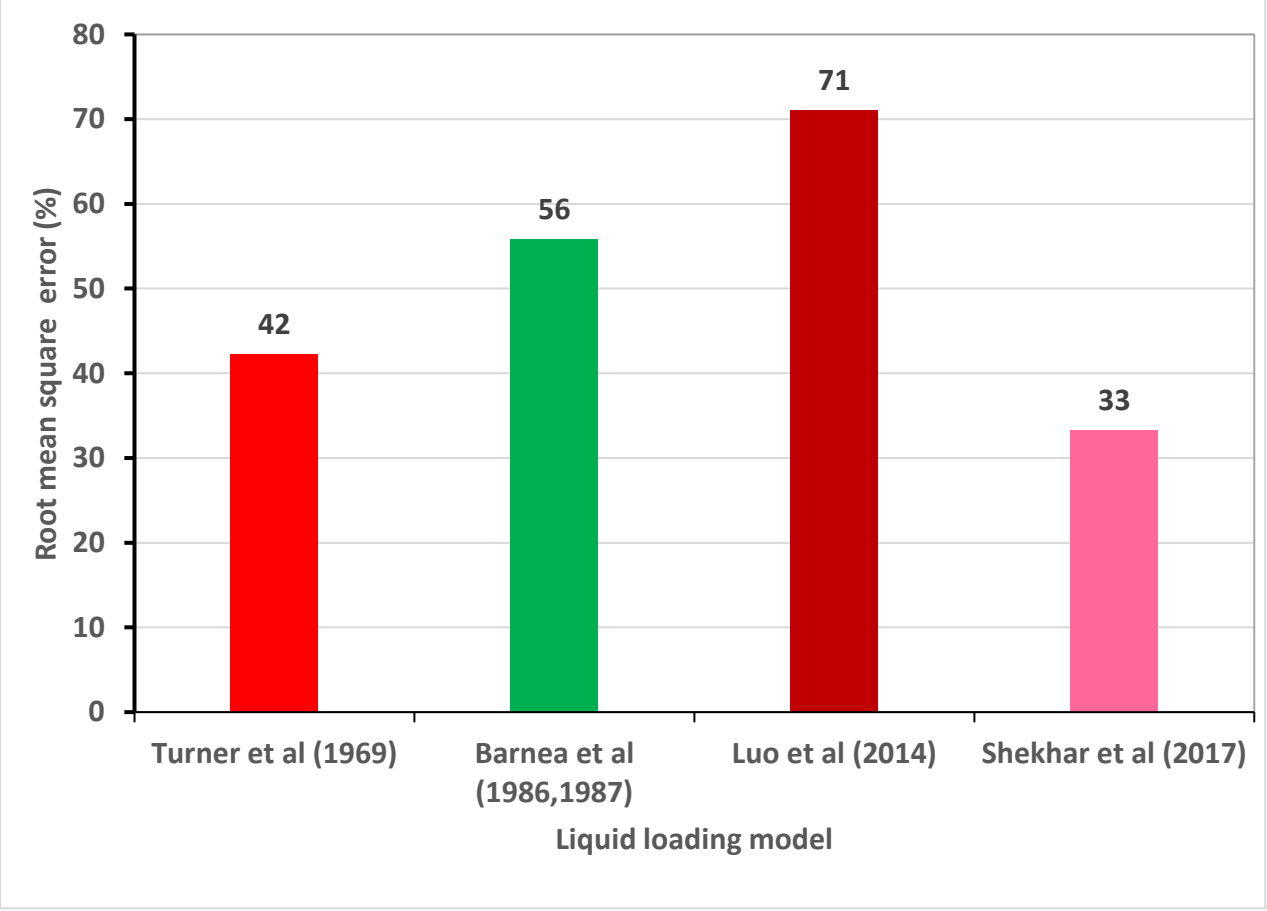

Fig. 4.9 - Comparison of model accuracy in predicting liquid loading using Veeken et al (2010) data.

4.2 Effect of droplet entrainment in the model of Luo et al. (2014).

Film reversal models are derived considering the fact that, liquid is transported as film along the walls of the tubing. However, the turbulence nature of gas flow induces the shear force at the gas-liquid film interface resulting to the formation of liquid droplets that are transported in the gas core. The fraction of droplets entrained in the gas core depends on the relative velocity and the properties of the flowing fluid phases. Most of the existing film reversal models assumes that all liquid is transported in the form of film neglecting the droplets entrained in the gas core. This assumption has been found to over-estimate the film thickness as well as the calculated critical gas velocity.

In this section, the effect of droplet entrainment in the gas core in the Luo's model was examined. This was done by using Well-1 and Well-2 data published by Belfroid et al. (2008). The fraction of liquid droplets entrainment in the gas core (f_E) was varied from 0 to 1. When $f_E = 0$, the liquid flow is completely in film and when f_E is closer to 1, the liquid is transported as droplets entrained in the gas core. It was assumed that the total mass flow of liquid is conserved as the part of liquid film is converted to the droplets by the shear force acting on the liquid-gas interface. The plots of gas superficial velocity against f_E for both Well-1 and Well-2 are as shown below;

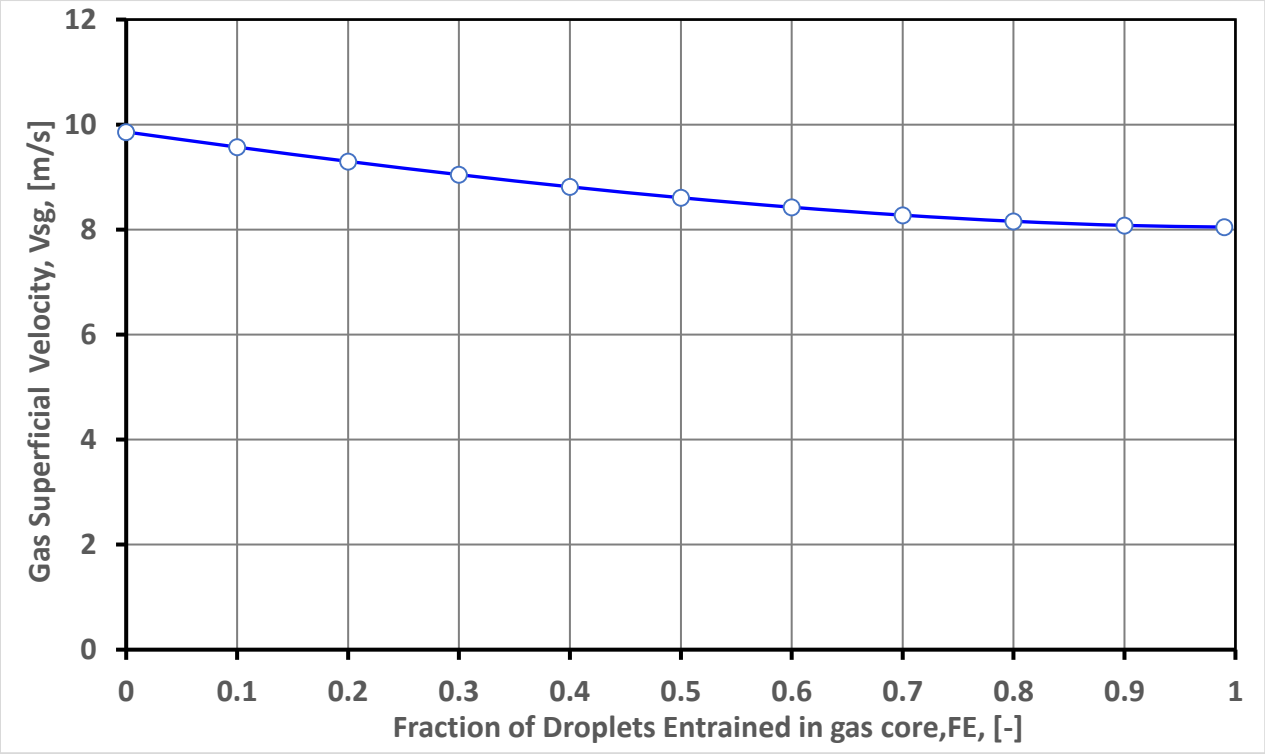

Fig. 4.10 - Effect of droplet entrainment in the gas core on critical V_{sg} for vertical well (WELL- 1)

The results presented in **Fig. 4.10** and **Fig. 4.11** shows that, as the fraction of droplets in the gas core increases from 0 to 1, the critical gas superficial velocity decreases accordingly. The decrease in gas superficial velocity with increasing f_E is triggered by the reduction in film thickness around the circumferential position of the pipe making easier for the liquid to be transported to the surface. Contingent to the magnitude of shear force induced at the gas-liquid film interface which controls the amount of droplets in the gas core, the critical velocity calculated without droplet entrainment can be up to approximately 18% higher than when the droplets entrainment is considered.

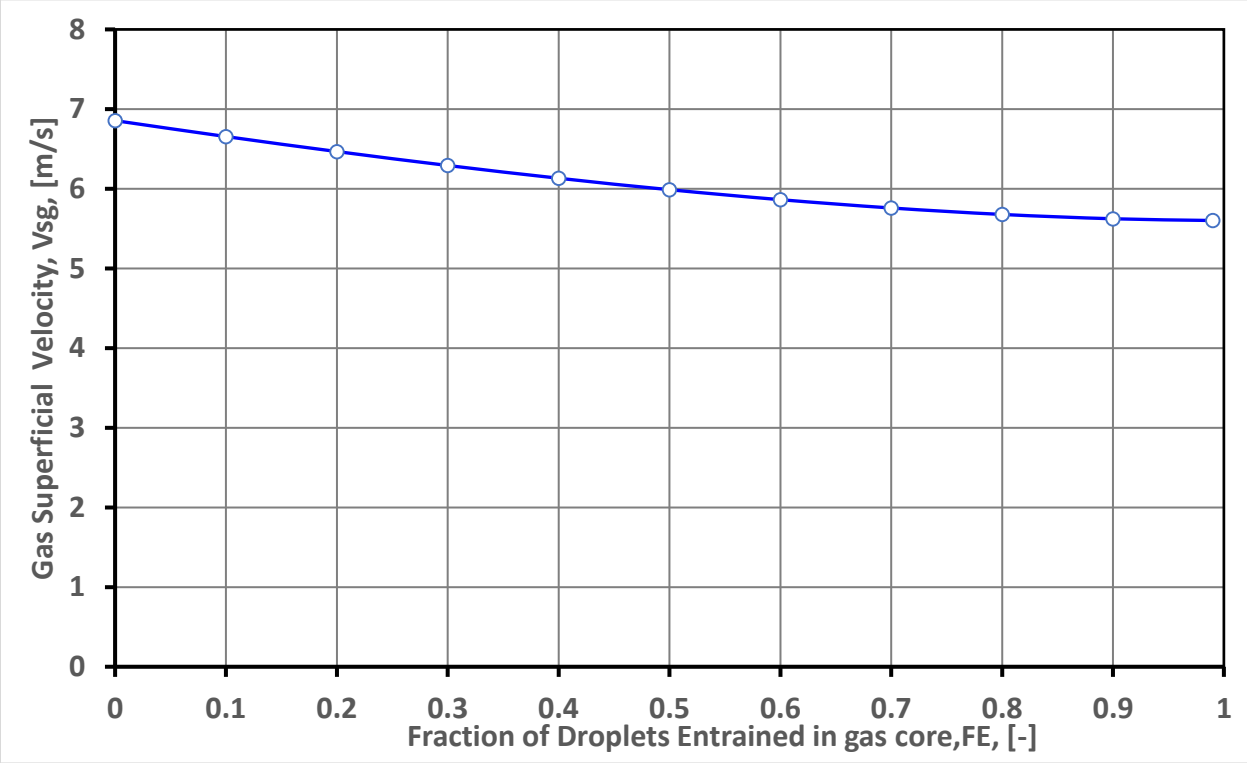

Fig. 4.11- Effect of droplet entrainment in the gas core on critical V_{sg} for vertical well (WELL- 2)

In addition, the effect of deviation angle of the pipe on gas superficial velocity for different fractions of liquid droplets entrainment was studied for both Well-1 and Well-2 from the data shared by Belfroid et al (2008). The trends of both **Fig. 4.12** and **Fig. 4.13** shows that, for the fraction of droplets entrainment in the range of 0 to 0.5, the gas superficial velocity increases as the inclination angle changes from 0° to 30° and decreases from 30° to 90°. These observations match with the experimental observations of Van't Westende (2008) which show that the maximum critical superficial gas velocity is observed at approximately 30° inclination angle. Under this condition, the film flow dominates the droplets flow and the flow pattern in the tubing is almost annular.

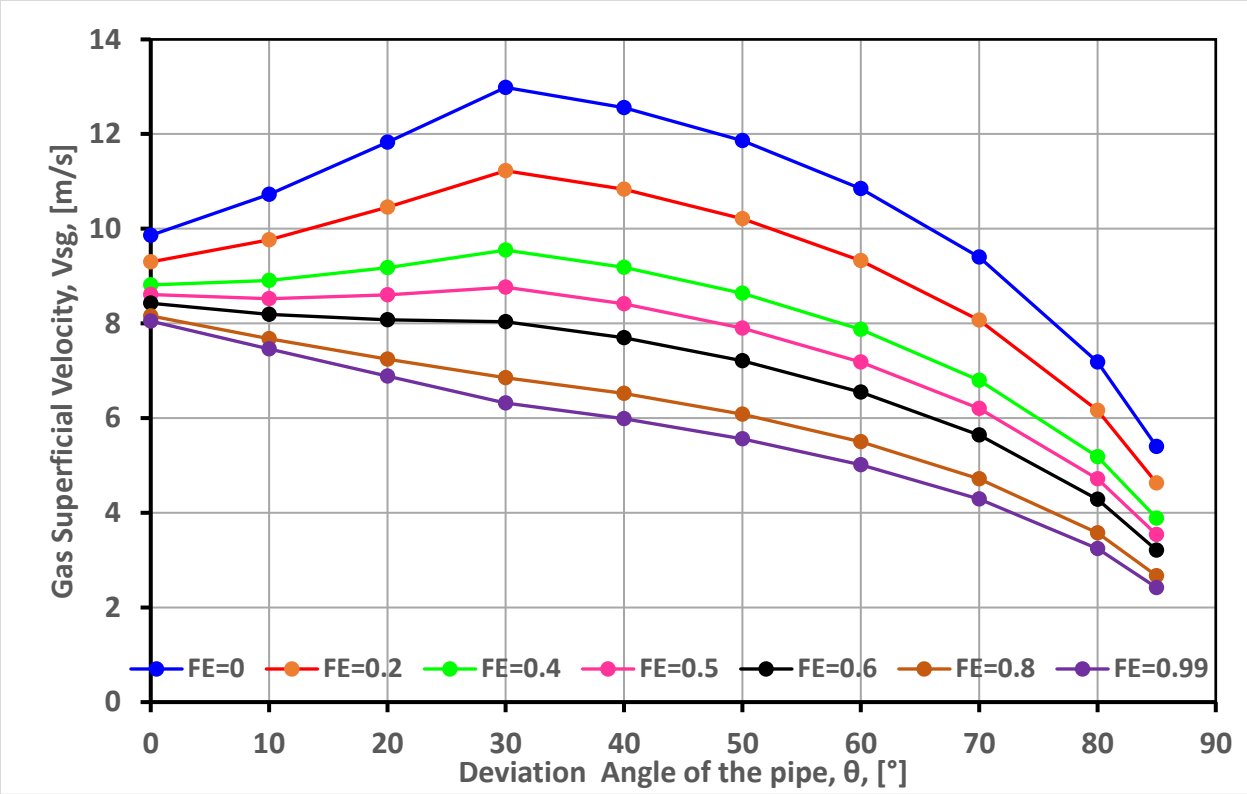

Fig. 4.12 - Effect of pipe deviation angle on gas superficial velocity at different fraction of droplets entrainment in the gas core (0° = Vertical) Well-1.

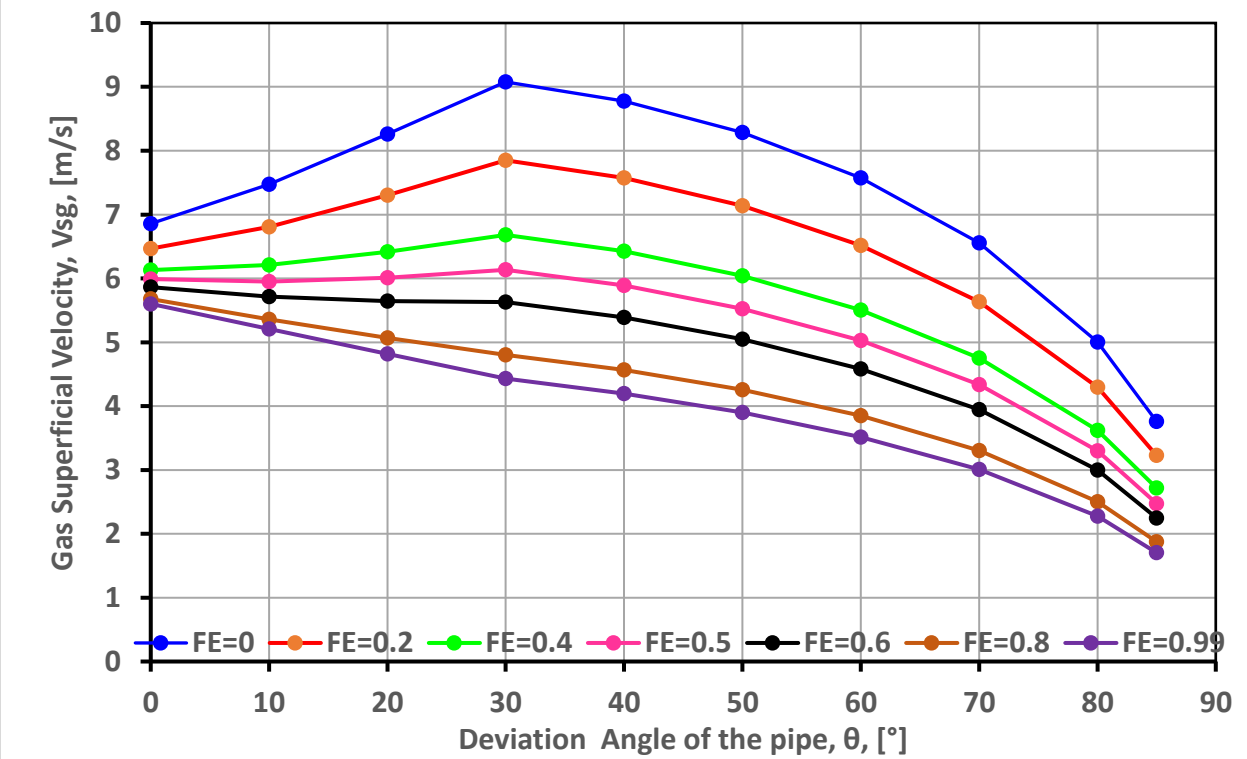

Fig. 4.13 - Effect of pipe deviation angle on gas superficial velocity at different fraction of droplets entrainment in the gas core (0° = Vertical) Well-2.

As the deviation angle of the pipe changes from 0° to 30°, the influence of thicker film thickness at the lower circumferential position of the pipe dominates the reduction in gravitational gradient and the overall consequence is the increase in critical superficial gas velocity. For deviation angle of the pipe in the range of 30º to 90º, the dramatic decrease in gravitational gradient dominates the effect of thicker film thickness at the bottom of the pipe thereby reducing the critical superficial gas velocity. At an inclination angle of 30° the difference in the critical gas velocity for the fraction of droplet entrainment between 0 and 1 is approximately 50%.

For the fraction of droplets entrainment above 0.5, the maximum gas superficial velocity is observed at an inclination angle of 0° (Vertical pipe) and minimum for nearly horizontal pipe. This is because the entrained droplets dominate the film flow and the flow pattern therefore change from **annular** to **mist** flow. Under this condition, the gravitational gradient remains the only factor affecting the critical superficial velocity. As the inclination angle changes from 0° to 90° under mist flow regime, the gravitational gradient of the fluid phases decrease requiring lower energy for the liquid to be transported to the surface. This is the reason for the prediction of critical gas superficial velocity to decrease continuously with increasing inclination angle of the pipe.

Based on the above observations, it is therefore important to consider the effect of droplets entrainment in the gas core to avoid the over-estimation of the critical superficial velocity in the film reversal models especially for high gas and liquid rate flowing wells. Luo et al. (2014) used the Wallis (1969) correlation defined in Eqn. (31) to compute the amount of droplet entrainment in the gas core at a given gas flow rate. The fraction of droplet entrainment estimated using this correlation is a function of gas superficial velocity and does not depend on the liquid superficial velocity. Using Belfroid et al (2008) well-1 data set, the superficial velocity map for the Luo et al. (2014) model with and without entrainment is shown in **Fig. 4.14.** By using the Wallis (1969) correlation, the estimated fraction of droplets entrainment in the gas core was 0.04 which was constant with increasing liquid flow rate. The superficial velocity map shows a minor deviation on the critical superficial velocity calculated using the Luo et al model with and without entrainment. This due to smaller amount of droplets entrainment estimated using the Wallis (1969) correlation and has negligible effect compared to the liquid film. Since the Wallis (1969) correlation lacks the dependence with respect to liquid flow rate, it results to under-estimation of the fraction of droplets entrained in the gas core especially when the liquid flow rate is high in the well. The correlation

can also result into large errors when the fraction of droplets entrainment is above 0.5 (Berna et al. 2015).

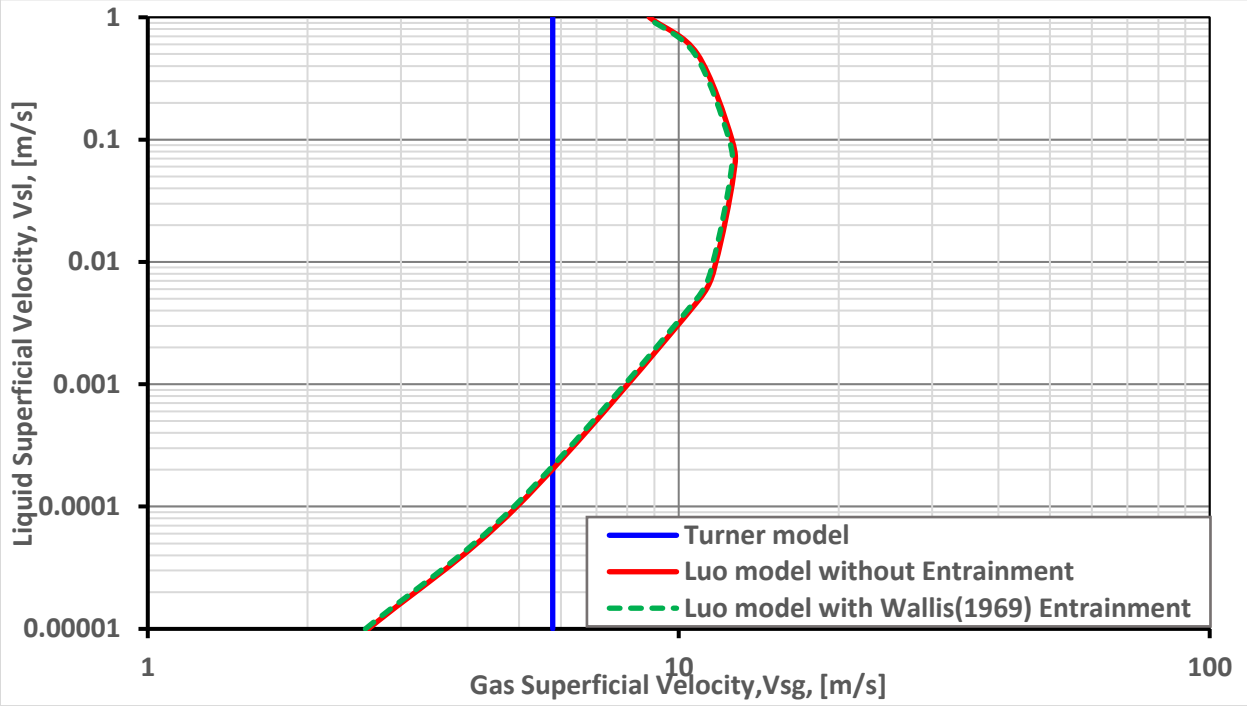

Fig. 4.14 - Superficial velocity map for the Luo et al (2014) model with and without entrainment.

To improve the prediction of entrainment, the correlations of Oliemans, et al. (1986) and (Ishii & Mishima, 1989) were used. These correlations capture the effect which the liquid flow rate has on the droplets entrainment. These correlations were then incorporated in the Luo, et al. (2014) model. The results shown in **Fig. 4.15** shows that, for liquid superficial velocity (V_{sl}) below 0.001m/s, there is a minor deviation on the superficial velocity curves estimated with and without droplets entrainment. For V_{sl} above 0.001m/s, the fraction of droplets entrainment estimated with both Oliemans, et al. (1986) and (Ishii & Mishima, 1989) increases. These observations are similar to those presented in **Fig. 4.10** and **Fig. 4.11** that the critical gas velocity decreases with the increase in the fraction of droplets entrainment. The maximum observed percentage deviation between the Luo et al. model without entrainment and with Oliemans, et al. (1986) entrainment correlation is up to 15% and 13% with (Ishii & Mishima, 1989) entrainment correlation. However, (Ishii & Mishima, 1989) entrainment correlation was derived using air/water data under low pressure in the range of 1-2.7 bar. This narrows the range of its appicability especially for wellhead pressures above 2.7 bar. Due to this fact, the (Ishii & Mishima, 1989) correlation was discarded.

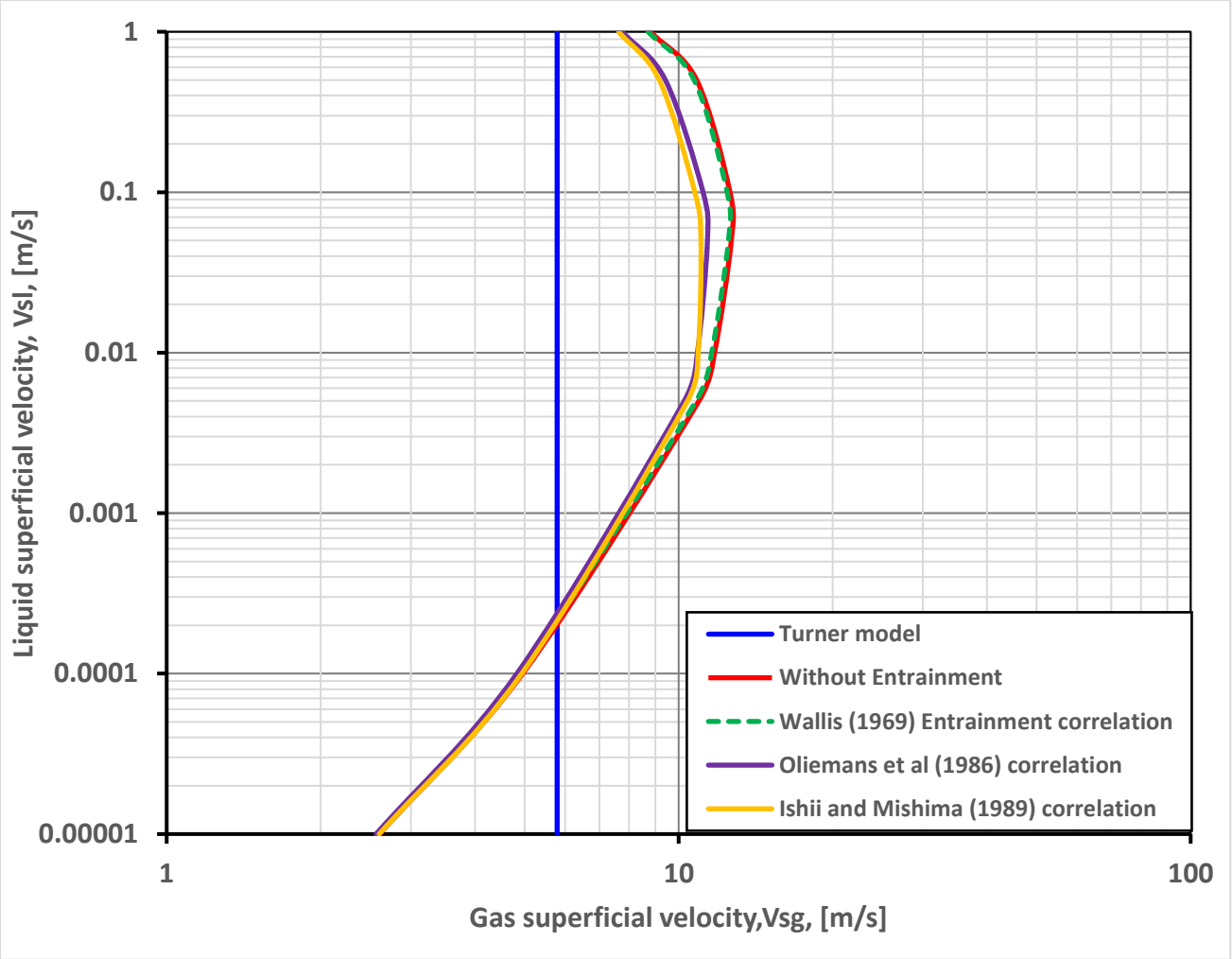

Fig. 4.15- Effect of entrainment correlation on the Luo et al 82014) model.

The Oliemans, et al. (1986) entrainment correlation was developed using the Harwell Databank with 727 data points consisting of air/water, steam, and hydrocarbon flows under pressures in the range of 1-100 bar. Due to its wide range of pressures and its ability to capture the effect of liquid flow rate, this correlation was recommended in the Luo et al. (2014) model instead of the Wallis(1969) entrainment correlation. This would reduce the over-prediction of the model up to 15% especially when the relative velocity between gas and liquid phases is high enough to dislodge more droplets at the gas- liquid film interface. The Oliemans, et al. (1986) and (Ishii & Mishima, 1989) entrainment correlations are shown in Eqn. (45) and Eqn. (46) respectively.

$$\frac{F_E}{1-F_E} = 10^{-2.52}\rho_l{}^{1.08}\rho_g{}^{0.18}\mu_l{}^{0.27}\mu_g{}^{0.28}\sigma^{-1.80}D^{1.72}V_{sl}{}^{0.70}V_{sg}{}^{1.44}g^{0.46} \qquad (45)$$

$$F_E = \tanh(7.25x10^{-7} {We_g}^{1.25} {R_l}^{0.25}) \quad (46)$$

Where We_g is the Gas Weber number defined by $We_g = \frac{\rho_g {V_{sg}}^2 D}{\sigma}\left(\frac{\rho_l - \rho_g}{\rho_g}\right)^{0.25}$ and Re_l is th the Liquid Reynolds numbe defined by $Re_l = \frac{\rho_g V_{sl} D}{\mu_l}$.

4.3 Effect of droplet entrainment in the Shekhar et al (2017) model

A comparison of the liquid loading models done in subsection 4.1.3 have revealed that the liquid film reversal model of Shekhar et al (2017) produces best results especially for deviated wells with large tubing sizes. Since the model was derived considering that all the liquid is transported as film along the walls of the tubing, the model was modified to include the effect of droplets entrainment. The Oliemans, et al. (1986) entrainment correlation was incorporated in the Shekhar et al. (2017) to see if the model prediction of the onset of liquid loading can be improved any further.

Based on the Veeken et al (2010) data, the critical gas superficial velocity was recomputed using Shekhar et al. (2017) with Oliemans, et al. (1986) droplet entrainment correlation. Upon including the entrainment correlation, the RMSE for the Shekhar et al. model was reduced from 33% to 29%. The performance of the model was compared to that of Luo et al (2014) with the same entrainment correlation, the RMSE from the Luo's model was found to decrease from 71% to 60% as shown in **Fig. 4.16**. However, the predictions from the Luo et al (2014) model are still conservative even after including the Oliemans, et al. (1986) droplet entrainment correlation . Lower RMSE value indicates that the Shekhar et al. (2017) model with the Oliemans, et al. (1986) droplet entrainment correlation can better predict the onset of liquid loading with greater accuracy than the original Shekhar et al. (2017) model, Turner et al (1969) model and the Luo et al. (2014) model with Wallis (1969) and Oliemans, et al. (1986) droplet entrainment correlations.

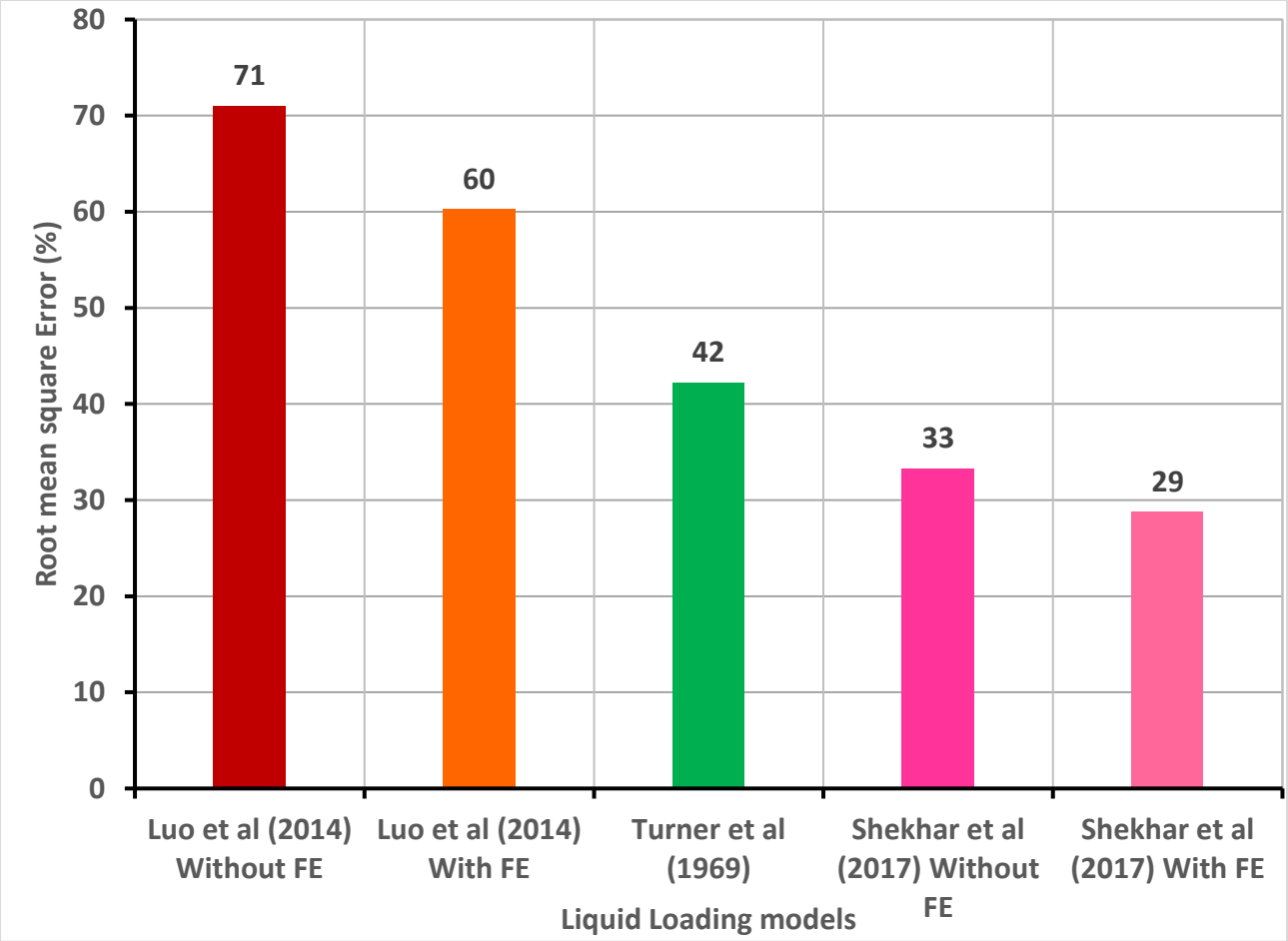

Fig. 4.16- Comparison of the liquid film reversal models with and without droplet entrainment.

4.4 Liquid loading criteria along the wellbore

4.4.1 Pressure traverse along the wellbore

In the literature, most of the calculations involving prediction of the onset of liquid loading are done considering the evaluation point to be the wellhead. This is because when the gas well is producing, it is easier to measure the pressure and temperature at the wellhead as compared to that at the bottomhole. Measurements of pressure at any position along the tubing requires pressure gauges to be placed at a point of interest in the wellbore. This process is usually complex and time consuming especially for acquiring subsurface data while the well is flowing. This is the reason for most of the researchers to make some simplification for using the wellhead as the evaluation point of the onset of liquid loading instead of the bottomhole. Another reason for choosing the wellhead as the evaluation point is the occurrence of highest gas velocity at the wellhead as compared to any other point in the well. For continuous unloading of liquid in the well, the gas

velocity must be greater than the critical velocity. For lower pressure wells, if it is possible to achieve this condition at the wellhead where there is highest velocity, then all other positions along the tubing will be free from liquid loading. However, for deeper positions in the tubing, the pressure will be higher, density is higher, local gas rates are lower and gas velocity is lower. Thus, there is a higher risk of having liquid loading lower in the tubing.

In this section the liquid loading criterial for different positions along the wellbore was evaluated. This was achieved by using the well data presented by (Zhou & Yuan, 2010) which are shown in **Table 4.2.** There is no any information about the loading status of this well which was indicated.

Table 4.2 - WELL A flowing conditions.

Parameter	**Value**	**Units**
Production rate	1659.5	Mscf/D
Perforation depth	8467	ft
Tubing depth	8410	ft
Tubing ID	2.441	in
Casing ID	4.780	in
Wellhead flowing pressure	1000	psig
Wellhead Temperature	110	°F
Bottomhole Temperature	166	°F
Gas Gravity	0.66	-
Water Gravity	1.07	-
Condensate Gravity	48	API
Water rate	10	bbl/MMscf
Condensate rate	10	bbl/MMscf

Using the well data presented in **Table 4.2**, the pressure drop calculation along the entire section of the wellbore was done by using (Gray, 1978) and (Beggs & Brill, 1973) correlations both programmed in excel VBA. The calculation procedures are as follows;

(i) The temperature gradient along the entire section of the wellbore was estimated using Eqn. (47) for a given wellhead and reservoir temperature assuming a constant temperature loss with depth.

$$\frac{dT}{dz} = \frac{T_R - T_{wh}}{\Delta z} \tag{47}$$

Where $\frac{dT}{dz}$ is the Temperature gradient [°F/ft], T_R is the reservoir temperature [°F], T_{wh} is the wellhead temperature [°F], Δz is the difference in elevation between the wellhead and the bottomhole depth [ft].

(ii) The entire section of the wellbore was then discretized into small segments of uniform or non-uniform length and the average temperature for each segment was calculated.

(iii) Departing from a segment with known pressure and temperature, a pressure drop (ΔP) between the end points of the considered segment was assumed (any guess is acceptable) and the average pressure of the segment was computed.

(iv) The required fluid properties such as fluid viscosities, fluid volume factors, gas compressibility factor and gas solubility were evaluated using average values of pressure and temperature at the mid-point of considered segment using correlations presented in **Table 8.1.**

(v) Using the detailed procedures described in **Appendix A** (for Gray correlation) and **Appendix B** (for Beggs and Brill correlation), the new value of ΔP was computed and compared to the previous value. If the difference between the new value and the previous values of ΔP does not fall within a pre-specified tolerance, the procedures are repeated with the previous value of ΔP replaced by the new value.

(vi) The procedures are repeated until when the difference between the new and the previous values of ΔP falls within a pre-specified tolerance. The convergence ΔP is accepted as the pressure drop in the considered segment.

(vii) The unknown pressure P_2 in the segment is then computed as $P_2 = P_1 + \Delta P$ if P_1 is a downstream pressure and $P_2 = P_1 - \Delta P$ if P_1 is the upstream pressure. The computed end node pressure P_2 in the current segment was then used as the input (P_1) to the next segment and the process were repeated in several segments until the end of the wellbore completion profile.

The resulting pressure profile for the entire length of the wellbore using both Gray (1978) and (Beggs & Brill, 1973) correlations is as shown in **Fig. 4.17**.

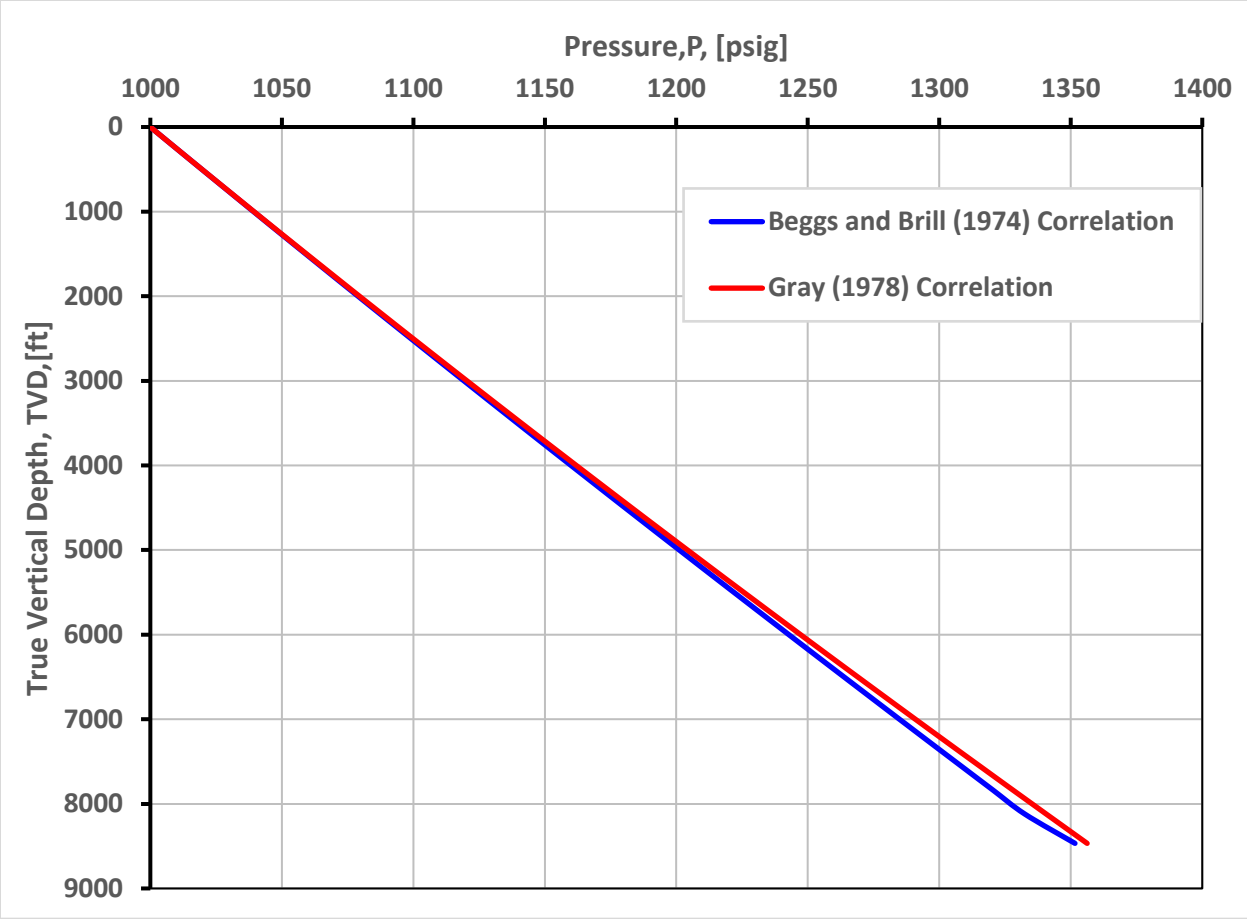

Fig. 4.17 - Pressure profile for WELL-A estimated using Gray (1978) and (Beggs & Brill, 1973) correlations.

The pressure profile calculated using both Gray (1978) and (Beggs & Brill, 1973) correlations shows a good match for well depth below 500ft and a minor deviation is observed for well depth above 500ft. The (Beggs & Brill, 1973) correlation checks for the flow pattern existing in every section assuming that the flow is horizontal. The liquid holdup is then corrected for other inclination angle of the pipe. This allows the flexibility in computation of friction and elevation gradient based on the flow patterns existing in the tubing. However, this correlation was derived for pipelines, it can over/under predict the pressure drop in vertical and deviated wells. Since WELL-A is vertical, a (Gray, 1978) correlation was adopted for calculating the pressure distribution along the entire section of wellbore. Gray (1978) correlation has been observed to provide good results in vertical wells especially for wells with condensate ratios up to 50 bbl/MMscf. The prediction from Gray (1978) correlation were therefore accepted as the better prediction for pressure profile for WELL A. The results of pressure profile obtained from Gray correlation programmed in excel VBA were compared to the pressure profile predictions from the

commercial software (**PROSPER** simulation software) using similar correlation containing its internal PVT models to see if they match. The pressure profile from Excel VBA and **PROSPER** software were observed to overlap as shown in Fig. **4.18** which indicate that the predictions from Excel VBA are accurate.

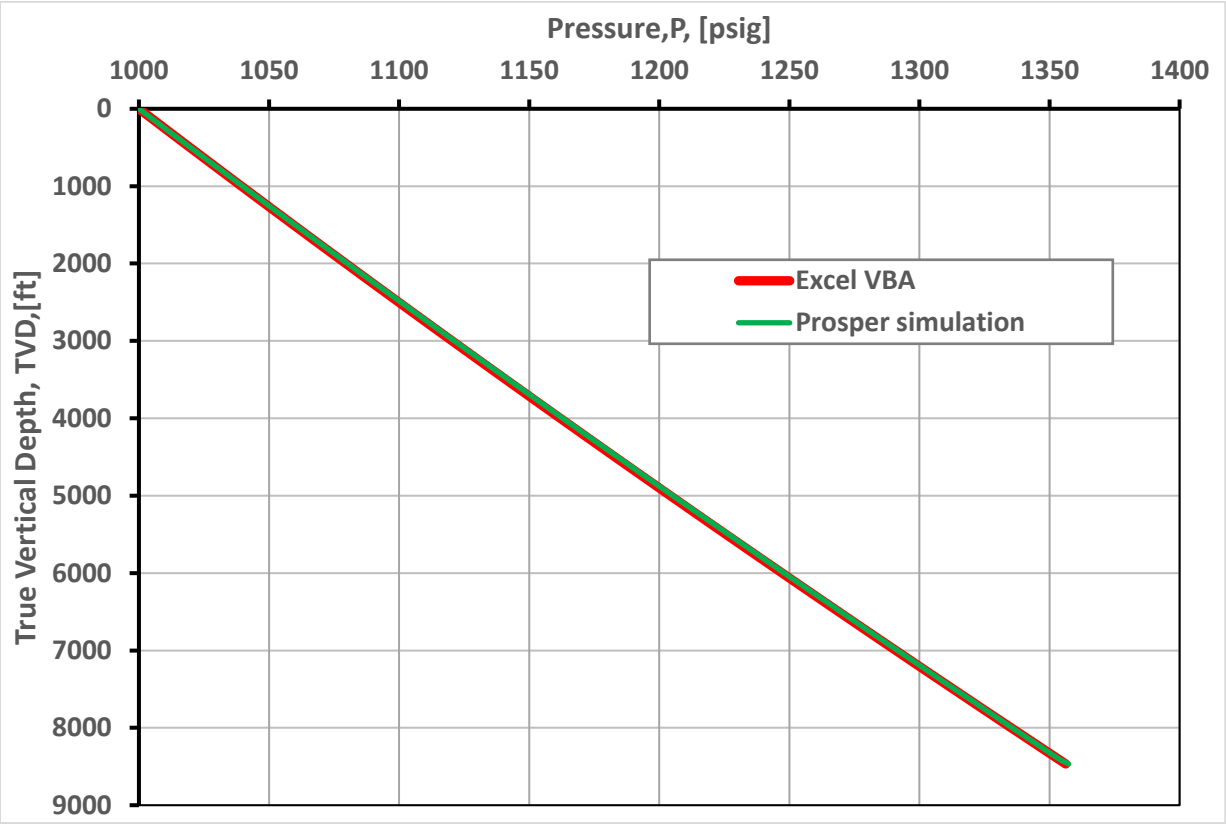

Fig. 4.18- Gray (1978) correlation pressure profile from Excel VBA and PROSPER simulation software

4.4.2 Evaluation of liquid loading condition along the wellbore

The pressure and temperature obtained from traverse calculations at all positions in the wellbore were used to compute the fluid volume factors (B_g, B_o *and* B_w) at every point in the wellbore. The reported standard conditions gas, condensate and water production rates were converted to in-situ (local) production rates using the relevant equations described in **Appendix A** (Eqn. A-12 and A-13). The gas and liquid superficial velocity were then computed by dividing the in-situ production rates to the cross-section area of the wellbore. The resulting liquid and gas superficial velocities were plotted against TVD as shown in **Fig. 4.19**. The gas superficial velocity was observed to decrease from *8.24ft/s* at the wellhead (0ft) to *6.87ft/s* at the end of the tubing depth (*8410ft*) and a dramatic decrease in V_{sg} from *6.87ft/s* to *1.78ft/s* in the perforation zone (*8410-8467ft*) due to

increase in diameter of the flow conduit from *2.441* to *4.78in*. On the other hand, the Liquid superficial velocity was observed to increase slightly from *0.072 ft/s* at the wellhead to *0.075ft/s* at the end of the tubing section. A dramatic decrease in V_{sl} from *0.075* to *0.02ft/s* was also observed in the perforated zone. The fact behind the decrease in V_{sg} and increase in V_{sl} from the wellhead to the bottomhole is due to condensation of some heavier gas components to liquid phase as the pressure and temperature increases with depth.

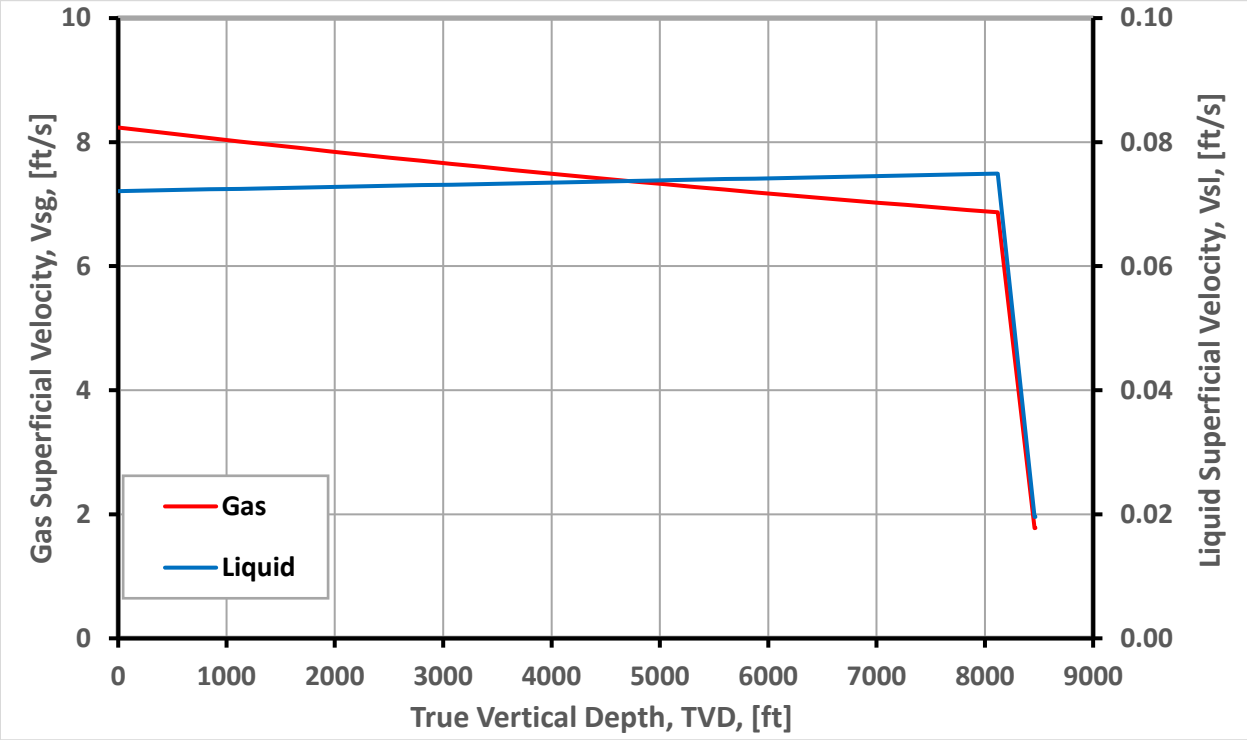

Fig. 4.19- Gas and Liquid superficial velocity trends along the wellbore (WELL A)

To evaluate the liquid loading criterial along the entire section of the wellbore, the liquid loading droplet model of Turner et al. (1989) and the modified film reversal models of Shekhar et al. (2017) were used to compute the critical gas velocity for vertical well. The resulting critical gas velocity ($V_{sg\_critical}$) from the loading models were compared to the current velocity (V_{sg_actual}) at every position in the wellbore. If it happen at any position in the tubing that V_{sg_actual} is greater than $V_{sg\_critical}$, the well is unloaded, otherwise the well is loaded up.

As it can be seen in **Fig. 4.20**, For the Turner's model $V_{sg\_actual} > V_{sg\_critical}$ along the tubing section and vice versa in the perforation zone. This indicates that the wells is unloaded along the entire section of the tubing while it is loaded in the perforation zone.

The predictions from the modified Shekhar et al. (2017) model shows that the well is unloaded from the wellhead to the well depth of approximately 1000 ft since $V_{sg\_critical} < V_{sg\_actual}$ and then changes to loaded status for the well depth greater than 1000 ft. Therefore, in order to come up with a precise conclusion that the well is loaded or unloaded, it is very important to evaluate the liquid loading status of the well at both the wellhead and the bottomhole. The well will be unloaded only if at any position of the tubing the critical gas superficial velocity calculated from the loading models is less than the current gas superficial velocity observed in the tubing, otherwise the well will be loaded up.

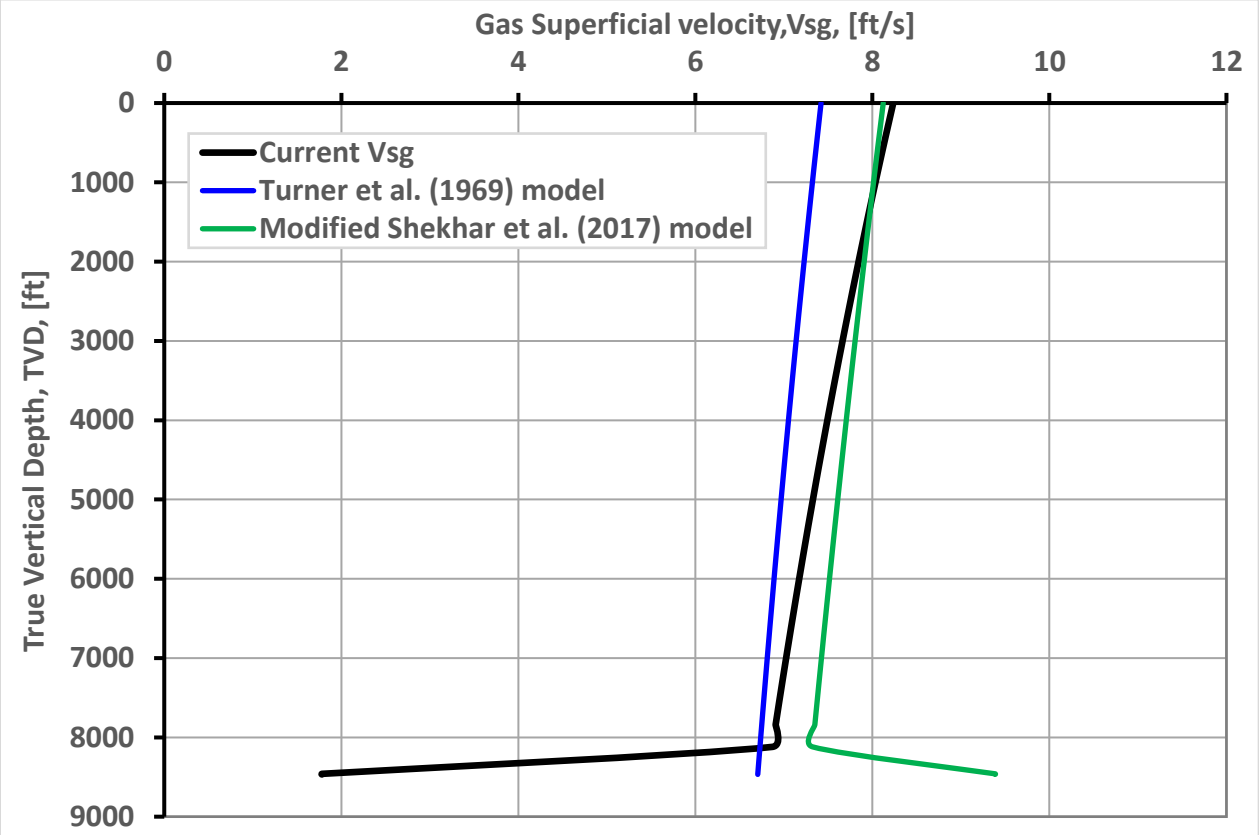

Fig. 4.20 - Liquid loading status along the entire section of the wellbore for vertical well.

Similar calculations were repeated for a gas well with deviation angles of 10°, 30° and 60° from the vertical as shown in **Fig. 4.21**. The results from the Turner's model shows a similar trend since it is independent of the deviation angle of the well. Therefore, for all deviation angle of the tubing, the predictions shows that the well is unloaded along the tubing section and loaded up along the perforation zone.

The results from the modified Shekhar et al. (2017) model for all deviation angles of the pipe (except for vertical pipe) shows that the well is loaded along the entire section of the tubing and the perforation zone. At 30° deviation angle of the pipe, the model predicts the highest critical gas velocity as compared to any other deviation angle of the pipe.

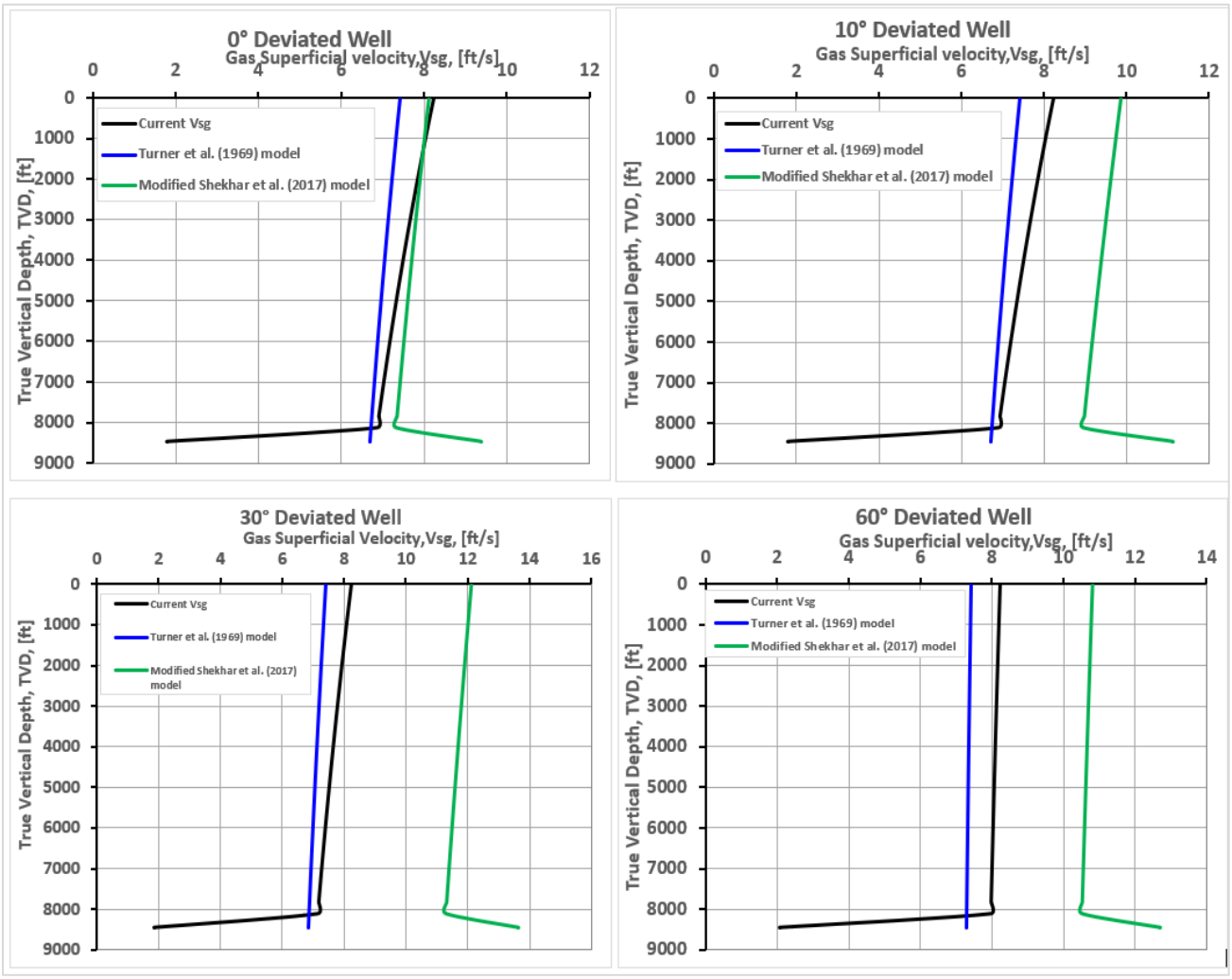

Fig. 4.21: Evaluation of liquid loading status for gas well with deviation angle of 0°, 10°, 30° and 60° from the vertical

5.0 CONCLUSION AND RECOMMENDATIONS

5.1 CONCLUSION

Upon comparing the liquid droplet reversal model of Turner et al. (1969) and the liquid film reversal models of Barnea (1986,1987), Luo et al. (2014) and Shekhar et al. (2017), the following conclusions can be drawn.

1. The Turner's model can predict with a good accuracy (up to 100%) the loading condition and status of the vertical wells producing under unloaded conditions. However, the model was found to under-estimates the critical flow rate for wells producing under loaded conditions.
2. The liquid film reversal model of Shekhar et al. (2017) was observed to better predict the critical gas velocity for the deviated wells with large diameters in the range of 2 to 6 inches as compared to other film reversal models of Barnea and Luo et al. (2014).
3. The study on the effect of droplet entrainment in the film reversal models have revealed that the critical velocity can be over-predicted by up to 18% if the liquid is regarded to be flowing as a film around the walls of the pipe and neglecting the effect of droplets entrainment in the gas core which is a result of liquid film dislodge by the shear force occurring at the gas-liquid film interface.
4. Based on the Veeken et al. (2010) field data, the use of the Oliemans et al. (1986) instead of Wallis (1969) entrainment correlation in the Luo et al. (2014) was observed to reduce the Root mean square error (RMSE) by 15%. Despite these improvements, the Luo's model still over-predicts the critical gas velocity.
5. The Shekhar et al. (2017) model was modified to include the (Oliemans et al. 1986) droplets entrainment correlation, the RMSE was found to decrease by 12% as compared to the Original Shekhar et al. (2017) model. The modified Shekhar model was therefore observed to better predict the onset of liquid loading than all other models compared under this study.
6. The study on the liquid loading criterial along the entire section of the well using the Turner and the modified Shekhar et al. (2017) model have revealed that, the evaluation point of the onset should be done at both the wellhead and the bottomhole so that a precise conclusion of whether the well is loaded or unloaded can be derived.

5.2 RECOMMENDATIONS

The following recommendations were suggested.

1. The film reversal models are based on the fact that liquid loading occurs immediately after the transition from annular to slug flow. Further experimental studies should be done to investigate the effect transition from annular to other flow patterns if they have similar effect to the slug flow.
2. Though the modified Shekhar et al (2017) model was found to better predict the onset of liquid loading as compared to other models, the RMSE was still significant. Further studies on the friction factor and the droplet entrainment correlation should be done to further increase the model accuracy.
3. The evaluation point of the onset of liquid loading should be done at both the wellhead and the bottomhole. Therefore, proper selection of the correlations used for pressure traverse calculations along the pipe is required to match with the conditions of the well.

6.0 NOMENCLATURE

Symbol	Meaning	SI units	Field units
D	Pipe diameter	m	inch
f_o	Fraction of condensate in total liquid	-	-
f_w	Fraction of water in total liquid	-	-
f_E	Fraction of droplets entrained in gas core	-	-
g	Acceleration due to gravity	m/s^2	ft/s^2
g_c	Gravitational conversion constant	Kgm/Ns^2	$lbm\text{-}ft/lbf\text{-}s^2$
P	Pressure	bara	psia
P_{sc}	Pressure at standard conditions	bara	psia
q_g	In situ gas flow rate	m^3/D	Mcf/D
$q_{\bar{g}}$	Gas flow rate at standard conditions	Sm^3/D	Mscf/D
q_O	In situ Condensate flow rate	m^3/D	Mcf/D
$q_{\bar{O}}$	Condensate flow rate at standard conditions	Sm^3/D	Mscf/D
q_w	In situ water flow rate	m^3/D	Mcf/D
$q_{\bar{w}}$	Water flow rate at standard conditions	Sm^3/D	Mscf/D
q_l	Total liquid in situ flow rate	m^3/D	Mcf/D
T	Temperature	bara	psia
T_{sc}	Temperature at standard conditions	°C	°F
V_g	In situ gas velocity	m/s	ft/s
V_l	In situ liquid velocity	m/s	ft/s
V_{sg}	Gas superficial velocity	m/s	ft/s
V_{sl}	Liquid superficial velocity	m/s	ft/s
Z	Gas compressibility factor	-	-
ρ_g	Gas density	Kg/m^3	lbm/ft^3
ρ_l	Liquid density	Kg/m^3	lbm/ft^3
ρ_o	Condensate density	Kg/m^3	lbm/ft^3
ρ_w	Water density	Kg/m^3	lbm/ft^3
θ	Inclination angle of the pipe from the horizontal	Degrees	Degrees
σ_o	Surface tension of condensate	N/m	dynes/cm
σ_w	Surface tension of water	N/m	dynes/cm
δ	Liquid film thickness	m	inch
$\bar{\delta}$	Dimensionless liquid film thickness	-	-
$\tilde{\delta}_T$	Dimensionless critical film thickness	-	-
$\tilde{\delta}_{avgl}$	Average dimensionless Film thickness	-	-

Abbreviations

GRL	Gas Liquid Ratio
RMSE	Root mean square error (%)
TVD	True vertical depth
VBA	Visual Basic for Applications
WHFP	Wellhead Flowing Pressure

7.0 REFERENCES

Oliemans, R. V., Pots, B. F., & Trompé, N. (1986). Modelling of annular dispersed two-phase flow in vertical pipes. *International Journal of Multiphase Flow, 12*(5), 711 - 732. doi:https://doi.org/10.1016/0301-9322(86)90047-9

Abdulmouti, H. (2014). Bubbly Two-Phase Flow: Part I- Characteristics, Structures, Behaviors and Flow Patterns. *American Journal of Fluid Dynamics, 4*(4), 194-240. doi:10.5923/j.ajfd.20140404.03

Asheim, H. (2017). Production wells. *Multi phase flow*.

Azzopardi, B. J. (2002). Multiphase flow. *Chemical Engineering and Chemical Process Technology, 1*.

Barnea, D. (1986). Transition from annular flow and from dispersed bubble flow—unified models for the whole range of pipe inclinations. *International Journal of Multiphase Flow, 12*(5), 733 - 744. doi:https://doi.org/10.1016/0301-9322(86)90048-0

Barnea, D. (1987). Transition from annular flow and from dispersed bubble flow—unified models for the whole range of pipe inclinations. *International journal of multiphase flow, 13*(1), 1 - 12. doi:https://doi.org/10.1016/0301-9322(87)90002-4

Beggs, D. H. (1984). *Gas Production Operations.* OGCI Publications Oil & Gas Consultants International Inc. Tusla.

Beggs, D. H., & Brill, J. P. (1973). A Study of Two-Phase Flow in Inclined Pipes. *Journal of Petroleum Technology - SPE-4007-PA, 25*(05). doi:10.2118/4007-PA

Beggs, H. D., & Robinson, J. R. (1975). Estimating the Viscosity of Crude Oil Systems. *Journal of Petroleum Technology, 27*(09). doi:https://doi.org/10.2118/5434-PA

Belfroid, S., Schiferli, W., Alberts, G., Veeken, C. A., & Biezen, E. (2008). Predicting Onset and Dynamic Behaviour of Liquid Loading Gas Wells. *SPE-115567-MS*. doi:https://doi.org/10.2118/115567-MS

Berna , C., Escrivá , A., Muñoz-Cobo , J. L., & Herranz, L. (2015). Review of droplet entrainment in annular flow: Characterization of the entrained droplets. *Progress in Nuclear Energy, 79*, 64 - 86. doi:https://doi.org/10.1016/j.pnucene.2014.11.011

Binli, Ö. (2009). *Overviw of Solutions to Prevent Liquid Loading in Gas wells.*

Bolujo, E. O., Fadairo, A. S., Ako, C. T., Orodu, D. O., Omodara, O. J., & Emetere, M. e. (2017). A New Model for Predicting Liquid Loading in Multiphase Gas Wells. *International Journal of Applied Engineering Research, 12*(14), 4578- 4586.

Coleman, S. B., Clay, H. B., McCurdy, D. G., & Norris III, L. H. (1991). A New Look at Predicting Gas-Well Load-Up. *43*(03). doi:10.2118/20280-PA

Cullender, M. H., & Smith, R. V. (1956). Practical Solution of Gas-Flow Equations for Wells and Pipelines with Large Temperature Gradients. *Petroleum Transactions, AIME, 207*, 281-287. Retrieved from https://www.onepetro.org/general/SPE-696-G

Darzi , M., & Park, C. (2017). Experimental Visualization and Numerical Simulation of Liquid-Gas Two-Phase Flows in a Horizontal Pipe. *ASME 2017 International Mechanical Engineering Congress and Exposition*. doi:10.1115/IMECE2017-72113

Duggan, J. O. (1961). Estimating flow rates required to keep gas wells unloaded. *Journal of Petroleum Technology, 13*(12), 1-173. doi:https://doi.org/10.2118/32-PA

Duns, H. J., & Ros, N. C. (1963). Vertical flow of gas and liquid mixtures in wells. Retrieved from https://www.onepetro.org/conference-paper/WPC-10132

Fabre, J. ,. (2015). *Slug flow*. doi:10.1615/AtoZ.s.slug_flow

Falcone, G., Hewitt, G., & Alimonti, C. (2009). *Multiphase Flow Metering; Principles and Applications* (1st ed., Vol. 54). Elsevier Science.

Fancher, G., & Brown, K. E. (1963). Prediction of Pressure Gradients for Multiphase Flow in Tubing. *3*(1). doi:10.2118/440-PA

Fore, L. B., Beus, S. G., & Bauer, R. C. (2000). Interfacial friction in gas–liquid annular flow: analogies to full and transition roughness. *International Journal of Multiphase Flow, 26*(11), 1755 - 1769. doi:https://doi.org/10.1016/S0301-9322(99)00114-7

Gao, Z.-K. K., Jin, N. D., & Wang, W. X. (2014). Definition of Flow Patterns. In *Nonlinear Analysis of Gas-Water/Oil-Water Two-Phase Flow in Complex Networks* (Vol. XIII). Springer. doi:10.1007/978-3-642-38373-1_2,

Gray, H. E. (1978). Vertical Flow Correlation in Gas Wells. *User's Manual for API 14B Surface Controlled Subsurface Safety Valve Sizing Computer Program*, (Appendix B).

Guo, B., & Ghalambor, A. (2005). *Natural Gas Engineering Handbook.* Houston Texas: Gulf Publishing Company.

Hagedorn, A. R., & Brown, K. E. (1965). Experimental Study of Pressure Gradients Occurring During Continuous Two-Phase Flow in Small-Diameter Vertical Conduits. *Journal of Petroleum Technology*. doi:https://doi.org/10.2118/940-PA

Hall, K., & Yarborough, L. (1973). new equation of state for Z-factor calculations. *Oil and Gas Journal, 71*(25), 82-92.

Hernandez, A. (2017). *Understanding the basics of liquid loading*. Retrieved from IHS Markit.

Hinze, J. O. (1955). Fundamentals of the hydrodynamic mechanism of splitting in dispersion processes. *AIChE Journal, 1*, 289-295.

Ishii, M., & Mishima, K. (1989). Droplet entrainment correlation in annular two-phase flow. *International Journal of Heat and Mass Transfer, 32*(10), 1835 - 1846. doi:https://doi.org/10.1016/0017-9310(89)90155-5

Katz, D. L., Cornell, D., Kobayashi, R., Poettmann, F. H., Varry, J. A., Elenbaas, J. R., & Weinaug, C. F. (1959). *Handbook of Natural Gas Engineering.* McGraw-Hill.

Kelkar, M., & Sarica, C. (2015). *Gas Well Pressure Drop Prediction under Foam Flow Conditions.* RPSEA.

Koperna, G. J. (2004). *Review and Selection of Velocity Tubing Strings for Efficient Liquid Lifting in Stripper Gas Wells.* Contracted work, Advanced Resources International, Inc.

Kumar, R. (2010). Two phase flow patterns and flow maps. *INDO –GERMAN WINTER ACADEMY- INDIAN INSTITUTE OF TECHNOLOGY*.

Lea, J. F., Nickens, H. V., & Wells, M. R. (2011). *Gas well deliquification* (2nd ed.). Gulf Professional Publishing.

Lee, A. L., Gonzalez, M. H., & Eakin, B. E. (1966). The Viscosity of Natural Gases. *Journal of Petroleum Technology, 18*(08). doi:https://doi.org/10.2118/1340-PA

Li, M., Sun, L., & Li, S. (2001). New View on Continuous-removal Liquids from Gas Wells. *Southwest Petro Ins and the CNPC Key Lab for Special Gas Reservoir Development*. doi:https://doi.org/10.2118/70016-MS

Luo, S. (2013). New Comprehensive Equation to Predict Liquid Loading. doi:10.2118/167636-STU

Luo, S., Kelkar, M., Pereyra, E., & Sarica, C. (2014). A New Comprehensive Model for Predicting Liquid Loading in Gas Wells. *29*(04). doi:10.2118/172501-PA

McCain, W. D. (1990). *The properties of petroleum fluids* (2nd ed.). Tusla, Oklahoma: PennWell Publishing Company.

Mukherjee , H., & Brill , J. P. (1985). Pressure Drop Correlations for Inclined Two-Phase Flow. *Journal of Energy Resources Technology, 107*(04). doi:10.1115/1.3231233

Nosseir, M., Darwich, T., Sayyouh, M., & El Sallaly, M. (2000). A New Approach for Accurate Prediction of Loading in Gas Wells Under Different Flowing Conditions. *SPE-66540-PA, SPE Production & Facilities, 15*(04). doi:https://doi.org/10.2118/66540-PA

Oden, R. D., & Jennings, J. W. (1988). Modification of the Cullender and Smith Equation for More Accurate Bottomhole Pressure Calculations in Gas Wells. *Permian Basin Oil and Gas Recovery Conference*. doi:https://doi.org/10.2118/17306-MS

Orkiszewski, J. (1967). Predicting Two-Phase Pressure Drops in Vertical Pipe. *Journal of Petroleum Technology- SPE-1546-PA, 19*(06). doi:10.2118/1546-PA

Perez, H. V. (2007). *Gas-liquid two-phase flow in inclined pipes.* PhD Thesis, University of Nottingham, School of Chemical Environmental and Mining Engineering. Retrieved from http://eprints.nottingham.ac.uk/11764/1/Hernandez-Perez.pdf

Poettman, F. H., & Carpenter, P. G. (1952). The Multiphase Flow of Gas, Oil, and Water Through Vertical Flow Strings with Application to the Design of Gas-lift Installations. *API-52-257*. doi:https://www.onepetro.org/conference-paper/API-52-257

Riza, M. F., Hasan, A. R., & Kabir, C. S. (2016). A Pragmatic Approach to Understanding Liquid Loading in Gas Wells. *SPE Production \& Operations*, 185-196.

Shekhar, S., & Kelkar, M. (2016). Prediction of Onset of Liquid Loading in Vertical, Inclined and Near Horizontal Wells. *SPE-181244-MS, SPE North America Artificial Lift Conference and Exhibition*. doi:https://doi.org/10.2118/181244-MS

Shekhar, S., Kelkar, M., Hearn, W. J., & Hain, L. L. (2017). Improved Prediction of Liquid Loading In Gas Wells. *SPE-186088-PA, 32*(04). doi:https://doi.org/10.2118/186088-PA

Standing, M. B. (1981). *Volume and Phase Behavior of Oil Field Hydrocarbon Systems* (9th ed.).

Sutton, R. P., Cox, S. A., Lea, J. F., & Rowlan, O. L. (2010). Guidelines for the Proper Application of Critical Velocity Calculations. *SPE-120625-PA, SPE Production & Operations, 25*(02), 182-194. doi:https://doi.org/10.2118/120625-PA

Taitel , Y., Barnea , D., & Dukler, A. (1982). A film model for the prediction of flooding and flow reversal for gas-liquid flow in vertical tubes. *International Journal of Multiphase Flow, 8*, 1 - 10. doi:https://doi.org/10.1016/0301-9322(82)90002-7

Thiruvengadam , M., Armaly, B. F., & Drallmeier, J. A. (2009). Shear-driven liquid film in a duct. *Engineering Applications of Computational Fluid Mechanics, 3*(4), 506-513. doi:10.1080/19942060.2009.11015287

Turner , R. G., Hubbard , M. G., & Dukler, A. E. (1969). Analysis and Prediction of Minimum Flow Rate for the Continuous Removal of Liquids from Gas Wells. *21*(11). doi:10.2118/2198-PA

Veeken , K., Hu , B., & Schiferli, W. (2010). Gas-Well Liquid-Loading-Field-Data Analysis and Multiphase-Flow Modeling. *25*(03). doi:https://doi.org/10.2118/123657-PA

Wallis, G. B. (1969). One Dimensional Two-Phase Flow.

Westende, V. (2008). *Droplets in annular-dispersed gas-liquid pipe-flows.* Doctoral thesis, Delft Technical university, Delft, Netherlands. doi:uuid:3d8367ef-c426-4536-8bde-2c3498227acb

Westende, V. J., Kemp, H., Belt, R., Portela, L., Mudde, R., & Olieman, R. (2007). On the role of droplets in cocurrent annular and churn-annular pipe flow. *International journal of multiphase flow, 33*(6), 595 -615. doi:https://doi.org/10.1016/j.ijmultiphaseflow.2006.12.006

Zhang , H. Q., Wang, Q., Sarica, C., & Brill, J. P. (2003a). Unified model for gas-liquid pipe flow via slug dynamics—part 1: model development. *Journal of energy resources technology, 125*(4), 266 - 273.

Zhang , H. Q., Wang, Q., Sarica, C., & Brill, J. P. (2003b). Unified Model for Gas-Liquid Pipe Flow via Slug Dynamics—Part 2: Model Validation. *Journal of Energy Resources Technology, 125*, 787-810. Retrieved from http://dx.doi.org/10.1115/ETCE2002/PROD-29113

Zhang, P., Cheng, X., Liu, R., Yang, J., & Zheng, K. (2015). Abnormal liquid loading in gas wells of the Samandepe Gasfield in Turkmenistan and countermeasures. *2*(4), 341-346. doi:https://doi.org/10.1016/j.ngib.2015.09.007

Zhou, D., & Yuan, H. (2010). A New Model for Predicting Gas-Well Liquid Loading. *25*(02). doi:10.2118/120580-PA

8.0 APPENDICES

APPENDIX A:
Pressure traverse in the tubing by using Gray Correlations

The pressure gradient is given by

$$\frac{dp}{dz} = \frac{g\rho_m}{144g_c} + \frac{2f_{tp}{V_m}^2\rho_{ns}}{144g_cD} \quad \text{(A-1)}$$

The calculation procedures are as follows;

1. Discretize the flow string into finite number of segments and identify the midpoint of each segment.
2. Depart from a segment with known pressure and temperature and assume a value of pressure drop (ΔP) between the end points of a segment under consideration. Calculate the average pressure and temperature.

   $P_{av} = P_1 + \frac{\Delta P}{2}$ if P_1 is the downstream pressure (A-2)

   $P_{av} = P_1 - \frac{\Delta P}{2}$ if P_1 is the upstream pressure (A-3)

   $T_{av} = T_1 + \frac{dT}{dz} x \frac{\Delta Z}{2}$ where $\Delta z = z_2 - z_1$, $\frac{dT}{dz}$ is the temperature gradient. (A-4)
3. Using the correlations listed in **Table 8.1**, calculate the fluid properties R_s , B_o, B_w, B_g, μ_o, μ_w, μ_g and Z_g at the average pressure and Temperature (P_{av}, T_{av}).

Table 8.1 - Methods and Correlations used for Predictions of fluid properties

Parameter	Units	Correlation
R_s	scf/stb	(Standing, 1981)
B_o	[-]	(Standing, 1981)
μ_o	cp	(Beggs & Robinson, 1975)
B_w	[-]	(McCain, 1990)
μ_g	cp	(Lee et al. 1966)
B_g	[-]	Gas law
μ_w	cp	(Beggs & Brill, 1974)
Z_g	[-]	(Hall & Yarborough, 1973)

4. Calculate the Gas and Liquid density

   (i) $\rho_g = \frac{2.7\gamma_g P_{av}}{ZT}$ (A-5)

   (ii) $\rho_L = \rho_O f_o + \rho_w f_w$ (A-6)

   $f_o = \frac{q_{\bar{o}}}{q_{\bar{o}} + q_{\bar{w}}}$ (A-7)

   $f_w = 1 - f_o$ (A-8)

$$\rho_w = \frac{350\gamma_o + 0.0764 R_s \gamma_g}{5.615 B_o} \quad \text{(A-9)}$$

$$\rho_o = \frac{350\gamma_o + 0.0764 R_s \gamma_g}{5.615 B_o} \quad \text{(A-10)}$$

$$\gamma_o = \frac{141.5}{131.5 + API} \quad \text{(A-11)}$$

5. Calculate the in-situ gas and liquid flow rates

$$q_g = 1.16x10^{-2}\, q_{\bar{g}} B_g \quad \text{(A-12)}$$

$$q_l = 6.498x10^{-5}(q_{\bar{o}} B_o + q_{\bar{w}} B_w) \quad \text{(A-13)}$$

6. Calculate the in-situ liquid, gas and mixture superficial

$$A = \frac{\pi D^2}{4x144} \quad \text{(A-14)}$$

$$V_{sl} = {}^{q_l}/_{A} \quad \text{(A-15)}$$

$$V_{sg} = {}^{q_g}/_{A} \quad \text{(A-16)}$$

$$V_m = V_{sl} + V_{sg} \quad \text{(A-17)}$$

7. Calculate the Volumetric Liquid fraction (No slip Liquid holdup)

$$\lambda_L = \frac{V_{sl}}{V_m} \quad \text{(A-18)}$$

8. Calculate the non-slip density (ρ_{ns}) and the non-slip fluid viscosity (μ_{ns})

$$\rho_{ns} = \rho_L \lambda_L + (1 - \lambda_L)\rho_g \quad \text{(A-19)}$$

$$\mu_{ns} = \mu_L \lambda_L + (1 - \lambda_L)\mu_g \quad \text{(A-20)}$$

Where $\mu_L = \mu_o f_o + \mu_w f_w$

9. Determine the dimensionless variables, Velocity number (N1), Nominal diameter (N2), Ratio of liquid to gas superficial velocity.

$$N_1 = \frac{{\rho_{ns}}^2 {V_m}^4}{g\sigma(\rho_l - \rho_g)} \quad \text{(A-21)}$$

$$N_2 = \frac{gD^2(\rho_l - \rho_g)}{\sigma} \quad \text{(A-22)}$$

$$R_v = \frac{V_{sl}}{V_{sg}} \quad \text{(A-23)}$$

10. Calculate the in-situ Liquid holdup (E_L)

$$E_L = 1 - (1 - \lambda)(1 - e^{f_1}) \quad \text{(A-24)}$$

$$f_1 = -2.314 \left[N_1 \left\{ 1 + \frac{205}{N_2} \right\} \right]^{N_3} \quad \text{(A-25)}$$

$$N_3 = 0.0814 \left[1 - 0.00554 ln \left\{ 1 + \frac{730 R_v}{R_v + 1} \right\} \right] \quad \text{(A-26)}$$

11. Calculate the mixture (two-phase) density as;

$$\rho_m = \rho_L E_L + (1 - E_L)\rho_g \quad \text{(A-27)}$$

12. Calculation of friction pressure loss.

12.1. Calculate the effective roughness of the pipe (k_e)

$$k_e = \begin{cases} k^o, & R_v \geq 0.007 \\ k + R_v\left\{\dfrac{k^o - k}{0.007}\right\}, & R_v < 0.007 \end{cases} \quad \text{(A-28)}$$

$$k^o = \frac{28.5\sigma}{\rho_{ns} {V_m}^2} \quad \text{(A-29)}$$

12.2. Calculate the mixture Reynolds number

$$NR_{em} = \frac{\rho_m V_m D}{\mu_{ns}} \quad \text{(A-30)}$$

12.3. Use Chen (1979) equation to calculate the two-phase friction factor

$$f_{tp} = \left\{-2log\left[\frac{\varepsilon}{3.7065} - \frac{5.0452}{NR_{em}} log\left(\frac{\varepsilon^{1.1098}}{2.8257} + \frac{5.8506}{{NR_{em}}^{0.8981}}\right)\right]\right\}^{-2} \quad \text{(A-31)}$$

13. Calculate the pressure drop ΔP using the following equation.

$$\Delta P = \left(\frac{g\rho_m}{144 g_c} + \frac{2 f_{tp} {V_m}^2 \rho_{ns}}{144 g_c D}\right)\Delta Z \quad \text{(A-32)}$$

14. The calculated current ΔP is compared to the previous ΔP . If the different does not fall within a predefined tolerance, the procedures in step 2 to 13 are repeated with ΔP found in step 13 being the new pressure drop. If the difference falls within a pre-defined tolerance, the current ΔP is accepted and P2 is calculated as $P_1 \pm \Delta P$. These values are then used as inputs to the next segment and the process is repeated in a several segments until the end of the completion profile.

APPENDIX B:

Pressure traverse in the tubing by using Beggs and Brill Correlations

The pressure gradient is given by

$$\frac{\Delta P}{\Delta z} = \frac{\frac{g}{g_c}\rho_{tp} sin\theta + \frac{f_{tp}\rho_{ns}{V_m}^2}{2g_c D}}{1 - \frac{\rho_{tp} V_m V_{sg}}{g_c P_{av}}} \quad \text{(B-1)}$$

The calculation procedures are as follows;

1. Discretize the flow string into finite number of segments and identify the midpoint of each segment.
2. Depart from a segment with known pressure and temperature and assume a value of pressure drop (ΔP) between the end points of a segment under consideration. Calculate the average pressure and temperature.

   $P_{av} = P_1 + \frac{\Delta P}{2}$ if P_1 is the downstream pressure (B-2)

   $P_{av} = P_1 - \frac{\Delta P}{2}$ if P_1 is the upstream pressure (B-3)

   $T_{av} = T_1 + \frac{dT}{dz} x \frac{\Delta Z}{2}$ where $\Delta z = z_2 - z_1$, $\frac{dT}{dz}$ is the temperature gradient. (B-4)
3. Using the correlations listed in **Table 8.1**, calculate R_s , B_o, B_w, B_g, μ_o,μ_w, μ_g and Z_g at average values of pressure and Temperature P_{av}, and T_{av}

4. Calculate the Gas and Liquid density

   (iii) $\rho_g = \frac{2.7\gamma_g P_{av}}{ZT}$ (B-5)

   (iv) $\rho_L = \rho_O f_o + \rho_w f_w$ (B-6)

   $f_o = \frac{q_{\bar{o}}}{q_{\bar{o}} + q_{\bar{w}}}$ (B-7)

   $f_w = 1 - f_o$ (B-8)

   $\rho_w = \frac{350\gamma_o + 0.0764 R_s \gamma_g}{5.615 B_o}$ (B-9)

   $\rho_o = \frac{350\gamma_o + 0.0764 R_s \gamma_g}{5.615 B_o}$ (B-10)

   $\gamma_o = \frac{141.5}{131.5 + API}$ (B-11)
5. Calculate the in-situ gas and liquid and gas flow rates

   $q_g = 1.16x10^{-2}\, q_{\bar{g}} B_g$ (B-12)

   $q_l = 6.498x10^{-5}(q_{\bar{o}} B_o + q_{\bar{w}} B_w)$ (B-13)
6. Calculate the in-situ liquid, gas and mixture superficial

   $A = \frac{\pi D^2}{4x144}$ (B-14)

(B-15)

$$V_{sl} = {}^{q_l}/_{A} \quad \text{(B-16)}$$

$$V_{sg} = {}^{q_g}/_{A}$$

$$V_m = V_{sl} + V_{sg} \quad \text{(B-17)}$$

7. Calculate the Volumetric Liquid fraction (No slip Liquid holdup)

$$\lambda_L = \frac{V_{sl}}{V_m} \quad \text{(B-18)}$$

8. Calculate the two-phase Froude number (NFR) and Liquid velocity number (NLV)

$$N_{FR} = \frac{V_m^2}{gx\left(\frac{D}{12}\right)}, \qquad N_{LV} = 1.938 V_{sl}\left(\frac{\rho_L}{\sigma_L}\right)^{0.25} \quad \text{(B-19)}$$

Where

$$\sigma_L = \sigma_o f_o + \sigma_w f_w \quad \text{(B-20)}$$

9. Determine the flow pattern which would exist if the flow were horizontal

9.1.Calculate the limiting parameters

$$L_1 = 316\lambda_L{}^{0.302} \quad \text{(B-21)}$$

$$L_2 = 0.0009252\lambda_L{}^{-2.4684} \quad \text{(B-22)}$$

$$L_3 = 0.1\lambda_L{}^{-1.4516} \quad \text{(B-23)}$$

$$L_4 = 0.5\lambda_L{}^{-6.738} \quad \text{(B-24)}$$

9.2. Use the following limiting parameters to determine the flow pattern

Segregated:

$\lambda_L < 0.001$ and $N_{FR} < L_1$

Or

$\lambda_L \geq 0.001$ and $N_{FR} < L_2$

Transition:

$\lambda_L \geq 0.001$ and $L_2 \ < N_{FR} < L_3$

Intermittent:

$0.01 \leq \lambda_L < 0.4$ and $L_3 \ < N_{FR} \leq L_1$

Or

$\lambda_L \geq 0.4$ and $L_3 \ < N_{FR} \leq L_4$

Distributed:

$\lambda_L < 0.4$ and $N_{FR} \geq L_1$

Or

$\lambda_L \geq 0.4$ and $N_{FR} > L_4$

10. Calculate the horizontal holdup $H_L(O)$

$$H_L(O) = \frac{a\lambda_L{}^b}{N_{FR}{}^c} \quad \text{(B-25)}$$

11. Calculate the Inclination correction factor coefficient (C)

$$C = (1 - \lambda_L) Ln\left(d\lambda_L^e N_{LV}^f N_{FR}^g\right) \quad \text{(B-26)}$$

The constants a, b, c, d, e, f and g are dependent on the flow pattern as shown in Table 2.

12. Calculate the liquid holdup inclination correction factor

$$\psi = 1 + C[sin(1.8\theta) - 0.333sin^3(1.8\theta)] \quad \text{(B-27)}$$

Where θ is the deviation angle of the pipe from the horizontal axis

Table 8.2 - Flow pattern constants

Flow Pattern	a		b	c
Segregated	0.98		0.4846	0.0868
Intermittent	0.845		0.5351	0.0173
Distributed	1.065		0.5824	0.0609
	d	e	f	g
Segregated uphill	0.011	-3.768	3.539	-1.614
Intermittent uphill	2.96	0.305	-0.4473	0.0978
Distributed uphill	No correction	C= 0		
All flow pattern downhill	4.70	-0.3692	0.1244	-0.5056

13. Calculate the liquid holdup

For segregated, intermittent and distributed flow pattern,

$$H_L(\theta) = \psi H_L(O) \quad \text{(B-28)}$$

When the flow pattern is transition, the liquid holdup is taken as the average as follows;

$$H_{L\theta,transition} = (1 - B)H_{L\theta,segregate} + BH_{L\theta,Intermittent} \quad \text{(B-29)}$$

$$B = \frac{L_3 - N_{FR}}{L_3 - L_2} \quad \text{(B-30)}$$

14. Calculate the two-phase mixture density

$$\rho_{tp} = \rho_L H_{L\theta} + \rho_g(1 - H_{L\theta}) \quad \text{(B-31)}$$

15. Determine the no-slip Reynolds number (N_{Rens})

Non-slip fluid density

$$\rho_{ns} = \rho_L\lambda_L + (1 - \lambda_L)\rho_g \quad \text{(B-32)}$$

Non-slip fluid viscosity (lbm/ft-sec)

$$\mu_{ns} = 6.72 * 10^{-4}\left[\mu_L\lambda_L + (1 - \lambda_L)\mu_g\right] \quad \text{(B-33)}$$

Non-slip Reynold's number

$$N_{Rens} = \frac{\rho_{ns}V_m}{\mu_{ns}}\left(\frac{D}{12}\right) \quad \text{(B-34)}$$

16. Calculate the non-slip friction factor

$$f_{ns} = \left[2Log\left(\frac{N_{Rens}}{4.5223LogN_{Rens} - 3.8215}\right)\right]^{-2} \quad \text{(B-35)}$$

17. Calculate the parameter S

$$S = \frac{Ln(y)}{-0.0523 + 3.182Ln(y) - 0.8725[Ln(y)]^2 + 0.01853[Ln(y)]^4} \quad \text{(B-36)}$$

For $y \leq 1, y \geq 1.2$

Where $y = \frac{\lambda_L}{H_{L\theta}{}^2}$ (B-37)

For $1 < y < 1.2$, S is calculated from;

$$S = Ln(2.2y - 1.2) \quad \text{(B-38)}$$

18. Calculate the two-phase friction factor

$$f_{tp} = f_{ns}e^{S} \quad \text{(B-39)}$$

19. Determine ΔP using the equation

$$\Delta P = \left(\frac{\frac{g}{g_c}\rho_{tp} sin\theta + \frac{f_{tp}\rho_{ns}{V_m}^2}{2g_c D}}{1 - \frac{\rho_{tp}V_m V_{sg}}{g_c P_{av}}} \right) \Delta Z \quad \text{(B-40)}$$

20. The calculated current ΔP is compared to the previous ΔP . If the different does not fall within a predefined tolerance, the procedures in step 2 to 19 are repeated with ΔP found in step 19 being the new pressure drop. If the difference falls within a pre-defined tolerance, the current ΔP is accepted and P2 is calculated as $P_1 \pm \Delta P$. These values are then used as inputs to the next segment and the process is repeated in a several segments until the end of the completion profile.